Energetic evaluation of swing adsorption processes for CO_2 capture in selected MOFs and zeolites: effect of impurities.

Daniel Bahamon[1,2], Alejandro Díaz-Márquez[2], Pablo Gamallo[2] and Lourdes F. Vega[1,3*]

[1] *Alya Technology & Innovation. Centre de Promoció Empresarial. C/ Tres Creus, 236. 08203 Sabadell, Barcelona, SPAIN.*

[2] *Departament de Ciència de Materials i Química Física & Institut de Química Teòrica i Computacional (IQTCUB), Universitat de Barcelona, C/ Martí i Franquès 1, 08028 Barcelona, SPAIN.*

[3*] *Gas Research Center and Department of Chemical Engineering. Khalifa University of Science and Technology, The Petroleum Institute. PO Box 2533, Abu Dhabi, UAE.*

AUTHOR INFORMATION

Corresponding Author

E-mail address: lvega@pi.ac.ae (Lourdes F. Vega). Tel.: +97126075626.

ORCID

Daniel Bahamon: 0000-0001-5473-1202

Alejandro Díaz-Márquez: 0000-0003-0517-5144

Pablo Gamallo: 0000-0002-8531-8063

Lourdes F. Vega: 0000-0002-7609-4184

ABSTRACT: *We present a systematic computational study of Mg-MOF-74, CuBTC and zeolite 13X for CO_2 separation from multi-component flue gas mixtures. The impurities' impact was evaluated at the molecular level and process conditions. Adsorption isotherms and isosteric heats of adsorption of pure (CO_2, N_2, O_2, H_2O, SO_2 and NO_2) components, binary and ternary mixtures were obtained from Grand Canonical Monte Carlo simulations. Working capacities, purities, recoveries and exergetic performances were evaluated for VSA/PSA/TSA processes. Results show that NO_2 has a negligible effect in the studied range. For H_2O and SO_2 the energy requirements are reduced as the impurity content increases and recovery and purity increase up to an "optimal" point where a competition for CO_2 preferred adsorption sites produces a sharp drop in purity and the energetic index grows exponentially. The minimum energy requirement were obtained for TSA at a desorbing temperature of 443K in the three materials, with impurities of 1% H_2O for CuBTC, 0.5% H_2O for Mg-MOF-74 and 0.02% H_2O for 13X, obtaining values of 1.13, 0.55 and 0.58 GJ/tCO_2, respectively. Hybrid VTSA processes with impurities content in the feed mixture and CCS specifications achieve energy performances of 0.36 GJ/tCO_2 and 0.46 GJ/tCO_2 with Mg-MOF-74 and 13X, respectively. Mg-MOF-74 stands up as an attractive material for VTSA processes, presenting higher working capacities, purities and second-law efficiencies, with lower energy consumptions, also showing a better "buffer" behavior than zeolite 13X when trace impurities are present. This work represents the first*

quantitative assessment of the process performance of MOFs adsorbents in swing adsorption process for CO_2 capture considering impurities effects. Results reinforce the validity of molecular simulations for guiding the optimization of these processes.

KEYWORDS: post-combustion CO_2 capture; Mg-MOF-74 and CuBTC; zeolite; Monte Carlo simulation; impurities; swing adsorption processes.

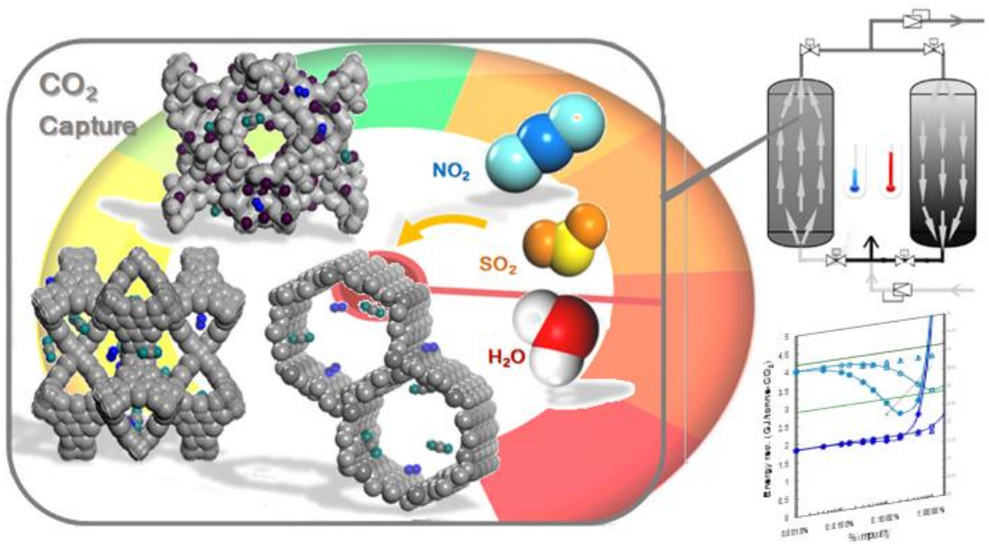

[Graphical abstract]

1. INTRODUCTION

In the context of sustainable development and clean energy production, one of the most important alternatives to mitigate anthropogenic CO_2 emissions is to capture and separate CO_2 (CCS) from diluted sources, such as gases emitted from fossil fuel combustion and other industrial processes.[1,2] CCS is already done at different industrial processes, depending on the targeted final use of the CO_2. In this sense, absorption by amine solvents has been long used in industry for gas removal due to the high CO_2 selectivity achieved at the chemisorption solvent process.[3] However, chemical absorption is an energy intensive process in which more than 30% of total energy is consumed for evaporation/thermal regeneration: the amine absorption/stripping technology from a conventional coal-fired power plant requires around 3-4 GJ_{th}/tonne-CO_2 [4] with an overall cost of the capture process between 51–82 US$/tonne-$CO_2$.[5] Besides, this process presents some disadvantages such as low contact area between gas and liquid, losses due to evaporation and tendency to induce corrosion and degradation in the presence of oxygenated compounds, among others.[6] Hence, finding alternative methods for efficiently separating CO_2 from a gas stream at a large scale remains an area of active research.

Among the alternative methods for CO_2 separation, the selective isolation of the gases near room temperature, known as Swing Adsorption Processes, can reduce the dependence of the less efficient energy processes in specialized applications and represents a revolutionary advance in order to achieve a more dynamic production at industrial level. These swing adsorption cycles have attracted a great attention since the theoretically minimum energy required for recovery of CO_2 from a flue gas and compression up to 150 bar is about 0.75 GJ/tonne-CO_2.[5]

In order to develop efficient adsorption processes, an appropriate adsorbent [7,8] should satisfy the following conditions: (1) high CO_2 adsorption capacity, (2) high CO_2 selectivity, (3) low heat capacity, (4) low-cost raw materials, (5) fast kinetics and (6) thermal, chemical, and mechanical stabilities under extensive cycling and impurities. A variety of solid adsorbents have been proposed to take into account structures and compositions, adsorption mechanisms and regeneration. Traditionally, both zeolites and activated carbons have been used for gas adsorption and separation. For instance, zeolite 13X provides high CO_2 adsorption capacity at room temperature although high energy requirements can be needed for the regeneration of the absorbent.[9]

Metal-Organic Frameworks (MOFs) have been one of the fastest growing fields in chemistry and materials science during the past decades, with the number of publications growing exponentially.[10] MOFs present a vast structural and chemical diversity, allowing potential applications in gas storage, ion exchange, molecular separation and heterogeneous catalysis,[11,12,13,14] as well as promising alternatives adsorbents for carbon dioxide capture application.[15,16,17]

The adsorption capacity of MOF materials at higher pressures is much greater than that observed in benchmark zeolite 13X. Several authors[18,19,20] have reported MOFs with high CO_2 adsorption capacity. Among them, CuBTC or HKUST-1 [$Cu_3(BTC)_2(H_2O)_3$, (BTC: benzene-1,3,5-tricarboxylate)], first reported by Chui *et al.*, [21] is one of the most studied MOFs for gas adsorption and storage. The reported CO_2 adsorption capacities are in the range between 8.0 mol/kg and 10.2 mol/kg at 298K and 15bar.[18,22] Differences are due to slightly different structural properties depending on the synthesis method.[23] An interesting contending, especially at lower pressures, is the so-called Mg-MOF-74.[24] This MOF currently displays one of the best adsorption performances for many gas molecules, with CO_2 uptakes as high as 8.1 mol/kg at 298 K and 1.0 bar. Such a high performance for

CO_2 capture is mainly attributed to strong interactions between CO_2 molecules and metal sites in the framework.[25,26]

A large number of MOFs studies have examined single-component CO_2 adsorption,[7,15] but limited amount of binary mixtures and multi-component calculations with MOFs have been published[27,28,29] providing limited data to be used for process design and integration at industrial conditions. In addition, only few studies have been devoted to the effect of moisture and/or impurities.[30,31,32,33,34,35,36,37,38] Those contaminants may significantly influence the performance of the adsorbent material.[39,40] For instance, Yazaydin *et al*. [30] reported CO_2 uptake and selectivity over N_2 and CH_4 in CuBTC, which significantly increased by the presence of water molecules coordinated to open-metal sites in the framework. Also, Liu *et al.* [28] studied adsorption equilibrium of CO_2/H_2O vapor and rates of CO_2 adsorption in CuBTC and Ni/DOBDC. Further efforts at understanding the effect of water on CO_2/N_2 separations in MOFs have more recently focused in Mg-MOF-74[25,41] with encouraging results related to its implementation in industrial processes. In addition, not only high CO_2 capacity, but also the resistance to flue gas components such as SO_2 and NO_x is quite important for a good sorbent for industrial applications.[31,32,37,42,43,44,45] However, to our knowledge, a systematic study on the effect of co-existing impurities in the mixture behavior and the quantitative evaluation of these changes in the energetic performance of the process under operational conditions has not been performed yet, which is the purpose of this work.

In general, and thanks to the high speed of today's computers, Grand Canonical Monte Carlo (GCMC) simulations can be used as a screening method for adsorption properties, providing valuable data such as uptakes, heats of adsorption and mixture behavior.[19,46,47] Hence, the goal of this study is to understand and quantify the influence of impurities on the energy requirements for capture and separation of CO_2 in post-

combustion mixture using CuBTC and Mg-MOF-74, compared to zeolite 13X. The election of these two MOFs is based on previous encouraging results obtained by us[48] and some other authors[24,28], and also on their commercial availability nowadays of these adsorbent materials. Zeolite 13X is used for comparison as a benchmark because of its industrial use[49].

The study has been performed in a systematic way. First GCMC simulations were used to evaluate adsorption capacities and isosteric heat distributions at an early stage of the process design. The force fields used for these simulations were conveniently validated with experimental data from literature in order to determine the accuracy of the model for pure components as well as the quality of the predictions for multicomponent mixtures. The effect of water and other coexisting impurities such as SO_2 and NO_2 traces in flue gas on CO_2 separation performance were quantified at different concentrations. Thus, the most suitable operating conditions for separation by swing adsorption processes for each material were found by calculating working capacities at process conditions, and complemented with energetic requirements evaluation. Finally, the VSA, PSA and TSA processes (and combinations of them) were compared and assessed based on equilibrium process parameters such as purity, recovery and exergetic analysis. Conclusions are presented in the final section.

2. METHODOLOGY

2.1. Adsorbent structures

Figure 1 shows a 2D projection of the crystallographic structures of the three adsorbents studied in this work: CuBTC, Mg-MOF-74 and zeolite 13X, generated for a

similar simulation box with dimensions ~30Å (size pores of the materials can be seen in Figure S1 of the Supplementary Material).

In the CuBTC framework, two octahedrally coordinated Cu atoms are connected to eight oxygen atoms of tetra-carboxylate units. Each benzene-1,3,5-tricarboxylate (BTC) ligand holds three Cu-paddle wheels forming two different microporous sites within the framework: a system of tetrahedral-shaped cages accessible through small windows (~3.5Å in diameter) and large cavities connected through square shaped windows with a diameter of ~9Å.[50] The partial positive charges on the metal sites in CuBTC are responsible for enhancing adsorption properties, as previously discussed in literature.[51,52]

Mg-MOF-74 (also known as CPO-27-Mg or Mg_2(DOBDC)), contains 2,5-dioxido-1,4-benzenedicarboxylate (DOBDC)[53] ligands and forms honeycomb-like structures with large one-dimensional pores of approximately 12Å diameter. Further, this MOF is based upon helical chains of an octahedral (consisting of Mg^{2+}−O coordination) that are located at the intersections of the honeycomb. Each Mg^{2+} ion in the structure bears an open-metal site, which is a highly favorable sorption site for various guest molecules.

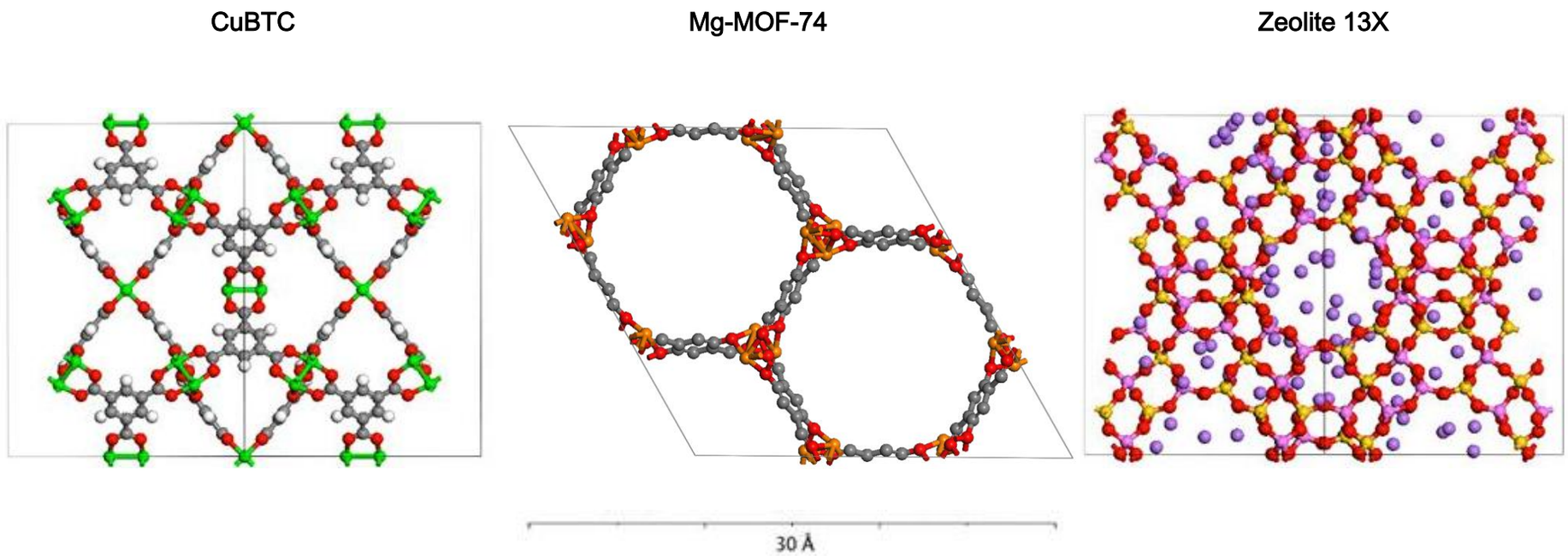

Figure 1. CuBTC (left), Mg-MOF-74 (center) and zeolite 13X (right) crystallographic structures. Red, gray, white, green, orange, yellow, pink and violet colors stand for oxygen, carbon, hydrogen, copper, magnesium, silicon, aluminum and sodium atoms, respectively.

Faujasite type zeolites are aluminosilicates classified as microporous materials with pore diameters between 6 and 12Å. Zeolite 13X, the most used faujasite structure has a molecular formula $[Si_{104}Al_{88}O_{384}]^{-88}Na^{+88}$ for its crystal structure. Depending of the desired adsorption and catalytic performance, Si/Al ratio can be altered by randomly replacing aluminum atoms by silicon,[54] but prohibiting Al-O-Al linkages in the zeolitic framework. The representative structure with Si/Al ratio = 1.18 (*i.e.*, 88 aluminum atoms per unit cell) is used in this work. It should be noted that most of the sodium atoms are located in pores with size diameter smaller than 6Å, keeping the other pores available for adsorption.

2.2. Simulation details

Molecular models for the three adsorbent materials were taken from single-crystal X-ray diffraction structures reported in literature: CuBTC reported by Chui *et al.,*[21] Mg-MOF-74 from NMR spectroscopy by Queen *et al*.[55] and zeolite 13X from Olson.[56]

The structures were replicated and orthogonalized to facilitate simulations and subsequent analysis. Solvent molecules were deleted, providing the so-called activated structures. All adsorption simulations were performed using GCMC techniques implemented in the Materials Studio[57] commercial software. GCMC simulations allows exchanging atoms or molecules with a reservoir at a constant temperature T, volume V and chemical potential μ.[58] Then, the amount of molecules adsorbed was calculated using a statistically averaged approach after the equilibrium stage for every single pressure point, allowing the construction of adsorption isotherms.

The common GCMC movements (*i.e*., insertions/deletions, translations and rotations) were attempted with equal probability to ensure microscopic detailed balance.

At each pressure (chemical potential) condition, $1.0\text{x}10^6$ MC moves were performed, $5.0\text{x}10^5$ to equilibrate the system and then additional $5.0\text{x}10^5$ MC moves were used for data collection ($1.0\text{x}10^7$ MC moves were used for simulations involving water). For more details on the implementations of the GCMC simulations for these types of studies the reader is referred to our previous work[48] and references therein.

All adsorbent frameworks, including the sodium cations of the zeolite, were treated as rigid structures with atoms fixed at their crystallographic positions. It should be noted that MOFs can be more flexible than zeolites, and several authors have explicitly considered the flexibility in their simulations.[59,60] Nevertheless, it has been found that rigid structures are appropriate when predicting adsorption of small gas molecules at non-extreme pressure conditions.[61]

A force field model for gas molecules was used with rigid geometrical structures, where only the nonbonded interactions were taken into account. Moreover, the pairwise interactions between the framework atoms have been excluded, since the structure was treated as frozen. Hence, the total energy of the system was calculated as the sum of the adsorbate-adsorbent and the adsorbate-adsorbate interaction energies at each step, modeled as a combination of Lennard Jones (LJ 12-6) and Coulomb potentials:

$$E_{ij} = 4\varepsilon_{ij}\left[\left(\frac{\sigma_{ij}}{r_{ij}}\right)^{12} - \left(\frac{\sigma_{ij}}{r_{ij}}\right)^{6}\right] + \frac{1}{4\pi\varepsilon_0}\frac{q_i q_j}{r_{ij}} \qquad (1)$$

where E_{ij} is the potential energy (or energy of interaction) between a pair of atoms i and j at a distance r_{ij}; q_i, q_j are the partial charge of atom i and j, respectively, ε_{ij} and σ_{ij} are the LJ potential well depth and diameter, respectively, and ε_0 is the vacuum permittivity.

Lennard-Jones parameters for zeolite and MOFs were taken from Watanabe *et al.*,[62] DREIDING[63] and UFF[64] force fields. Charges for CuBTC, Mg-MOF-74 and zeolite

13X atoms were obtained from the works of Castillo *et al.,*[33] Pham *et al.*[65] and Jaramillo *et al.* [66], respectively. Parameters for gas molecules were taken from the literature in a transferable manner, allowing accurate reproduction of the condensed phase properties.[67] CO_2, N_2 and O_2 were modeled using the TraPPE force field:[68] CO_2 molecules were modeled as rigid and linear. A linear three-site model was also used for the diatomic N_2 and O_2 molecules, with partial charges at the atoms and at the center of mass (fixed bond lengths of 1.16 Å, 1.10Å and 1.21Å for CO_2, N_2 and O_2 molecules, respectively). One of the most accurate models for water, the TIP-4P/2005 model,[69] was used to represent the H_2O molecule in order to evaluate the moisture effects in the mixture, while NO_2 and SO_2 molecules were modeled from the works of Ketko *et al.*[70] and Bourasseau *et al.*[71] respectively.

The full set of van der Waals parameters used is listed in Table S1 (See Supplementary Material). A cutoff radius of 12.5Å was applied to the Lennard–Jones interactions, and the long-range electrostatic interactions were calculated by using Ewald summation. Lorentz–Berthelot combining rules were used to calculate the adsorbate/framework and the Lennard–Jones crossed parameters, and the Peng-Robinson equation of state [72] was used to relate pressure with chemical potential.

The force fields were conveniently validated with adsorption isotherms experimental data from literature (when available) in order to determine the accuracy of the model for pure components adsorption isotherms calculated by GCMC (represented as excess amount adsorbed), as well as the quality of the multicomponent mixtures predictions.

2.3. Adsorption isotherms and related parameters

In addition to adsorption isotherms, GCMC simulations were also used to calculate other key properties for adsorption processes. The isosteric heat of adsorption, q_{ST}, is one of the most important thermodynamic quantities for understanding the thermal effects related to adsorption and the cost of desorption/regeneration. The isosteric heat depends on the surface coverage, and from energy/particle fluctuations using molecular simulations, q_{ST} can be calculated as: [73]

$$q_{ST} = RT - \frac{\langle E \times \mathcal{N} \rangle - \langle E \rangle \langle \mathcal{N} \rangle}{\langle \mathcal{N}^2 \rangle - \langle \mathcal{N} \rangle^2} \quad (2)$$

where E, $\mathcal{N}$ and R stand for the total potential energy of the system per molecule, the number of molecules adsorbed and the gas constant, respectively. The brackets $\langle ... \rangle$ denote an average in the GCMC ensemble.

Moreover, another very important property that is often used as evaluation criteria in Swing Adsorption processes is the working capacity (Δn_k) of the targeted component in the mixture. The working capacity is generally more relevant than the total uptake, since it determines the amount that can be recovered -for further use- at each adsorption/desorption cycle. This quantity is defined as:

$$\Delta n_k = n_{k,ads} - n_{k,des} \quad (3)$$

where k is the targeted component (*e.g.*, CO_2) and $n_{k,ads}$ and $n_{k,des}$ are the uptakes under adsorption and desorption conditions (*i.e.*, CO_2 from mixture at adsorption condition, and almost pure at desorption conditions). When the material is not highly selective for one component of the mixture -or the adsorbed composition is lowered due to poisoning by other component-, instead of simply using the amount removed from the adsorbent

material, $n_{k,des}$, from pure isotherms,[24,74] a good option is to multiply this pure isotherm for the adsorbed molar fraction, as implemented by Prats *et al*.[54]

2.3.1. Impurities

Whereas CO_2 and N_2 account for about 90% of the flue gas composition and can reach up to 95-97% before entering its final separation stage,[75] understanding the effect of traces gases is critical to properly evaluate any material for use in a realistic CO_2 capture process.[7,76] If these unwanted species are not completely removed in previous separation stages, they can compete for the adsorption sites on the adsorbent material and hence, the adsorption properties and final performance can be drastically affected. According to this, studies on the influence of coexisting trace compounds in the mixtures or possible "poisoning" of the adsorbent materials allow assessing the final performance of the material at process conditions, where these impurities may be present.

In order to quantify the effect of impurities on the performance of the selected materials for CO_2 capture, simulations were carried out maintaining a CO_2 composition of 15% in the flue gas and varying for different impurities compositions (nitrogen was used as the surplus). Concentrations as high as 1% (*i.e.*, 10,000 ppm) of H_2O, SO_2 and NO_2 in the mixture were evaluated in order to magnify the effect of these traces in the flue gas may be present due to inefficiencies in the previous removal systems.

2.4. Energy requirements for regeneration of the bed adsorber

One of the requirements for the industrial application of these materials is to have an effective and less energy-consumed regeneration of the CO_2 captured adsorbents. The most common regeneration techniques for swing adsorption processes include: (1) adsorb

at pressures above the atmospheric (PSA), (2) desorb at vacuum conditions (VSA) (3) desorb by increasing temperature (TSA) or (4) by using electricity (ESA), among others.[77] In order to assess the validity of the present study for practical applications, we provide next some insights into the understanding of the physical phenomena governing the behavior of the materials when adsorbing the different compounds present in the mixture, while including important equilibrium quantities often used as evaluation criteria in an early stage of design.[78]

The simplest configuration was considered for the swing adsorption process, including only two fixed beds in parallel, also called the 4-step Skarstrom's[79] cycle. While one bed is adsorbing, the other bed is desorbing (without including heat integration, pressure equalization and purge/rinse steps). The shortcut method described by Chung *et al*.[80] was adopted for the calculations, since it allows a simple description of PSA processes based only on equilibrium parameters obtained on the high and low pressure levels regardless of the rate. Chung *et al*.'s methodology is extrapolated to VSA and TSA processes in this study, serving as a screening tool in the early stage of the process design. Energy requirements for compression/vacuum, as well as for heating, were included as a way to represent the costs associated in the different processes. Global balances were performed at equilibrium adsorption and desorption conditions (non-differential, as the ones presented in the short-cut methods of Chan et al.[81] and Joss et al.[82]).

The adiabatic energy requirement for compression/vacuum was calculated in a similar way as Chaffee *et al*.[83] and Riboldi *et al*.[84] using the following equation:

$$W = \left(\frac{\gamma}{\gamma - 1}\right)\frac{(\theta)RT}{\eta}\left[\left(\frac{P_{ads}}{P_{des}}\right)^{\frac{\gamma-1}{\gamma}} - 1\right] \quad (4)$$

where η = 0.85 (compressor/blower efficiency), γ is the polytropic parameter (γ =1.28 and 1.40 for pure CO_2 and air, respectively), T is the temperature, P_{ads} is the pressure at adsorption conditions and P_{des} is the pressure at desorption conditions.

θ is the total number of moles where the work is effectuated, and varies from one process to the other. It should be noted that, depending on whether PSA or VSA processes are considered, the amount of pressurized or expanded substance differs. In VSA, the complete bed is subjected to a vacuum. Conversely, for PSA, the amount compressed will be higher and mainly depends on the working capacity of CO_2 at the feeding stream conditions, since purge/rinse has not been taken into account in this study. Hence, θ is calculated as follows for PSA and VSA processes:

$$\theta_{PSA} = \frac{\Delta n_{CO2}}{y_{CO2,feed}} \rho_S V(1-\epsilon)$$
$$\theta_{VSA} = \sum_k n_{k,ads} \rho_S V(1-\epsilon) \quad (5)$$

A value for void fraction of ϵ = 0.4 (*i.e.*, ϵ = (bulk density)/(framework density)) was used and a bed volume V of 1 m^3. When comparing among different materials, both the total volume of the column and the fractional voidage were held constant. Therefore, the total mass of the adsorbents used is governed by the framework density of the adsorbent materials, ρ_S.

The thermal regeneration energy, $Q_{thermal}$, is the energy required for heating and desorption in TSA processes. This total thermal regeneration energy involves two main contributions: (i) the energy required to heat the adsorbent material, and (ii) the energy required to overcome the endothermic desorption process. This energy can be calculated as:[85,86]

$$Q_{thermal} = \left(C_P \Delta T + \sum_k \bar{q}_{ST_k} \Delta n_k \right) \rho_S V (1 - \epsilon) \quad (6)$$

where C_P and $\bar{q}_{ST_k}$ are the heat capacity of the adsorbent and the isosteric heat of adsorption, respectively. Note that $\bar{q}_{ST_k}$ is often expressed as an average value for the entire surface coverage; we have used different values in this work depending on the amount adsorbed in each adsorption and desorption condition. Therefore $\sum_k \bar{q}_{ST_k} \Delta n_k$ becomes $\sum_k \left(q_{ST_k ads} n_{k,ads} - q_{ST_k des} n_{k,des} \right)$. In addition, densities and heat capacities were held constant and taken from the work by Huck *et al*.[85]

Moreover, thermal energy and electrical energy have been compared based on exergetic -energy quality- analysis. In this case, since thermal energy can be supplied in a power plant by diverting steam from the power cycle (thus reducing the power generation of the plant), $Q_{thermal}$ must be multiplied by the Carnot efficiency and the efficiency of the gas turbine.[87,88]

Two additional equilibrium process parameters used in this work are recovery and purity: the first one is defined as the relationship between working capacity and the uptake, while purity is related to the working capacities of all components.

Furthermore, it is known that for transportation through a pipeline network, CO_2 product stream must be compressed above 150 bar,[89] which is generally accomplished through a multi-stage compressor train with intercooling to compress the stream. Transportation and injection costs have not been included as they are out the scope of the current study.

3. RESULTS AND DISCUSSION

Results presented are divided into three parts: (1) simulations for pure components, validating the force fields and providing insights into the adsorptive capacity of the materials (2) simulations for CO_2 in flue gas mixtures with and without impurities, assessing the effect of the impurities on the adsorption and selectivity, and (3) energetic performance calculations for different VSA/PSA/TSA conditions, quantifying the energetic requirement for each of the processes with the three materials and the specific impurities concentrations.

3.1. Adsorption behavior of pure gases

The accuracy of the force fields was first compared with experimental pure gas adsorption curves from literature.[9,23,24,28,30,90,91,92,93,94] As shown in the Supplementary Material (see Figures S2 to S4), GCMC simulations agree with the experimental results, validating the force fields used and the simulation procedure followed. Note that simulated adsorption isotherms were mainly validated with experimental data for pure CO_2, N_2, O_2 and water, while comparison with experiments was not completely performed for SO_2 and NO_2 due to lack of data.[34,44] All force fields were used in a transferable manner for multicomponent mixtures, the predictions made for SO_2 and NO_2 might involve uncertainties.

As can be inferred from Figures S2-S4 (Supplementary Material) pure adsorption isotherms in CuBTC and Mg-MOF-74 obtained with GCMC for water using the TIP-4P/2005 do not adjust as well as nitrogen and carbon dioxide to the experimental data, issue previous found by Bahamon and Vega[48] and Peng *et al*. [95] Nevertheless the TIP-

4P/2005 is, among the available models for water at this level of approximation, the one that best describes the liquid–vapor density curve and the critical water conditions, capturing what should be observed in adsorption processes when the material is saturated, and condensation becomes important. Hence, the comparison is good enough to provide more than qualitative trends in all cases, allowing elucidating the influence on the process under real operating conditions. In addition, note that water molecules were not fixed into the CuBTC structure in the simulations, as done in previous studies by some other authors.[30,33]

In terms of water stability, while CuBTC and Mg-MOF-74 were found to be highly stable in water vapor for some authors,[96,97,98] other studies have observed a decrease in their specific surface area or water capacity at certain range of operation,[41,99,100] However, this should not be a limitation for the study carried out here, as most of the water should be separated in an earlier stage (only traces will remain), and the working operation composition is very low, up to 1% in the feed stream.

Individual adsorption isotherms simulated for the studied compounds are provided in Figure 2. Values are presented in volumetric units as the true exchange between materials should not affect the dimensions of an operative adsorption column[27,48] (gravimetric comparison can be found in Figures S5 and S6 in the Supplementary Material). In order to make a realistic comparison for gas stream at process temperatures conditions, a stream at 313K (*i.e.* 40°C) was selected as the feed gas stream and these are the results presented from now on. As expected, the amount of CO_2 adsorbed is higher in MOFs at higher pressures. The low pressure range is beneficial for zeolites which more easily attract the quadrupole of CO_2. However when the operating pressure reaches values

above 5-10 bar, zeolite 13X shows lower uptake capacities than MOFs due to smaller pore volumes.

The two MOFs frameworks have clearly different adsorption behavior: for instance, CO_2 adsorption capacity for CuBTC shows poor performance at lower pressures but higher uptakes as the pressure increases (*e.g.*, note that the uptake around 5-10 is very similar than in zeolite 13X and Mg-MOF-74). In contrast, Mg-MOF-74 exhibits exceptional CO_2 storage capacity at low pressures and high pressures. It is known that N_2 and O_2 molecules present weak interactions with zeolites and these two MOFs,[31] awarding good selectivity towards CO_2. Contrarily to the previously discussed compounds, simulations for water adsorption show that zeolite 13X is a more hydrophilic adsorbent than CuBTC and Mg-MOF-74. However, H_2O adsorption reaches saturation in all three materials in the low pressure region, indicating a strong guest-host interaction for all of them. Moreover, it is also interesting to note that SO_2 uptakes are also higher in MOFs than in the zeolite, and all materials have similar volumetric capacities for SO_2 and CO_2 molecules at the highest pressure calculated in this work. A different effect is observed for NO_2, where weaker interactions with the materials as compared to carbon dioxide were observed.

Isosteric heats are related to the slope of the increasing part of the adsorption isotherms: a sharp increase at low pressures means high q_{ST} values, while a small q_{ST} value implies lower adsorption capacity for a given pressure, but better regeneration cost.[101] The calculated isosteric heats of the pure components obtained by GCMC are comparable to those reported in literature: the simulated heats of adsorption in zeolite 13X were 39 kJ/mol for CO_2, 20 kJ/mol for N_2 and 82 kJ/mol for H_2O. The experimental heats of adsorption are in the range between 40 and 45 kJ/mol for CO_2,[7,9,18,24,102] and between 70

and 80 kJ/mol (*i.e.* 1500-1800 BTU/lb) for water.[103] The calculated $\bar{q}_{ST}$ values for CO_2, N_2 and H_2O in Mg-MOF-74 were 46, 21 and 78 kJ/mol respectively, in good agreement with results available in the literature[26,31,34] (45, 24 and 80 kJ/mol, respectively). Hence, a high similarity between zeolite 13X and Mg-MOF-74 with higher energy values is observed.

Regarding the other two trace impurities considered in this work, DFT-based calculated isosteric heats for SO_2[34] in Mg-MOF-74 suggest that our GCMC results underestimate SO_2 adsorption at low pressures (*e.g.*, a value of q_{st,SO_2}~ 75 kJ/mol, compared to our q_{st,SO_2} obtained of 58 kJ/mol). The same underestimation is observed for NO_2.[34] However, to our knowledge, there are no experimental data to make a direct comparison for these two impurity traces and the calculated values. Alternatively, CuBTC, shows an isosteric heat value for CO_2 30% lower than the one reported in zeolite 13X (*i.e.*, 25 kJ/mol) and higher capacities at higher pressures, becoming very attractive when regeneration costs are included in the study. A compilation of the calculated isosteric heats of adsorption for all species in all three structures can be seen in Figures S7 and S8 in the Supplementary Material, together with a brief explanation on the property behavior depending on the specific molecular interactions.

Calculations of pure component behavior provide insights about how certain gas mixtures will behave, and hence, qualitative information can be extracted about the species that will imply more competitive effects when working with impurities. According to this, three different cases have been selected in this work: an impurity with much higher adsorption energy than CO_2 (*i.e.*, H_2O), other with a slightly higher energy of adsorption than CO_2 (*i.e.*, SO_2), and one that affects adsorption in a lesser extent (*i.e.*, NO_2). Although a prediction of the mixture behavior can be obtained by parametrization of the isotherms and the use of the Ideal Adsorbed Solution Theory (IAST),[104] the applicability of the IAST

would fail when preferential location at the intersections of framework are present,[105] as it is the case of zeolite 13X and Mg-MOF-74, two highly selective materials for CO_2-over-N_2. Besides, there are many factors in mixtures able to alter the expected results from IAST due to interactions of new particles competing to be adsorbed, and which may provoke inhibition problems or, contrarily, to enhance adsorption, as it happens with some gases. This is one of the advantages of using GCMC simulations, as they allow calculating interactions between molecules in a direct manner, where competitions for adsorption are explicitly included, as will be discussed in the next sections.

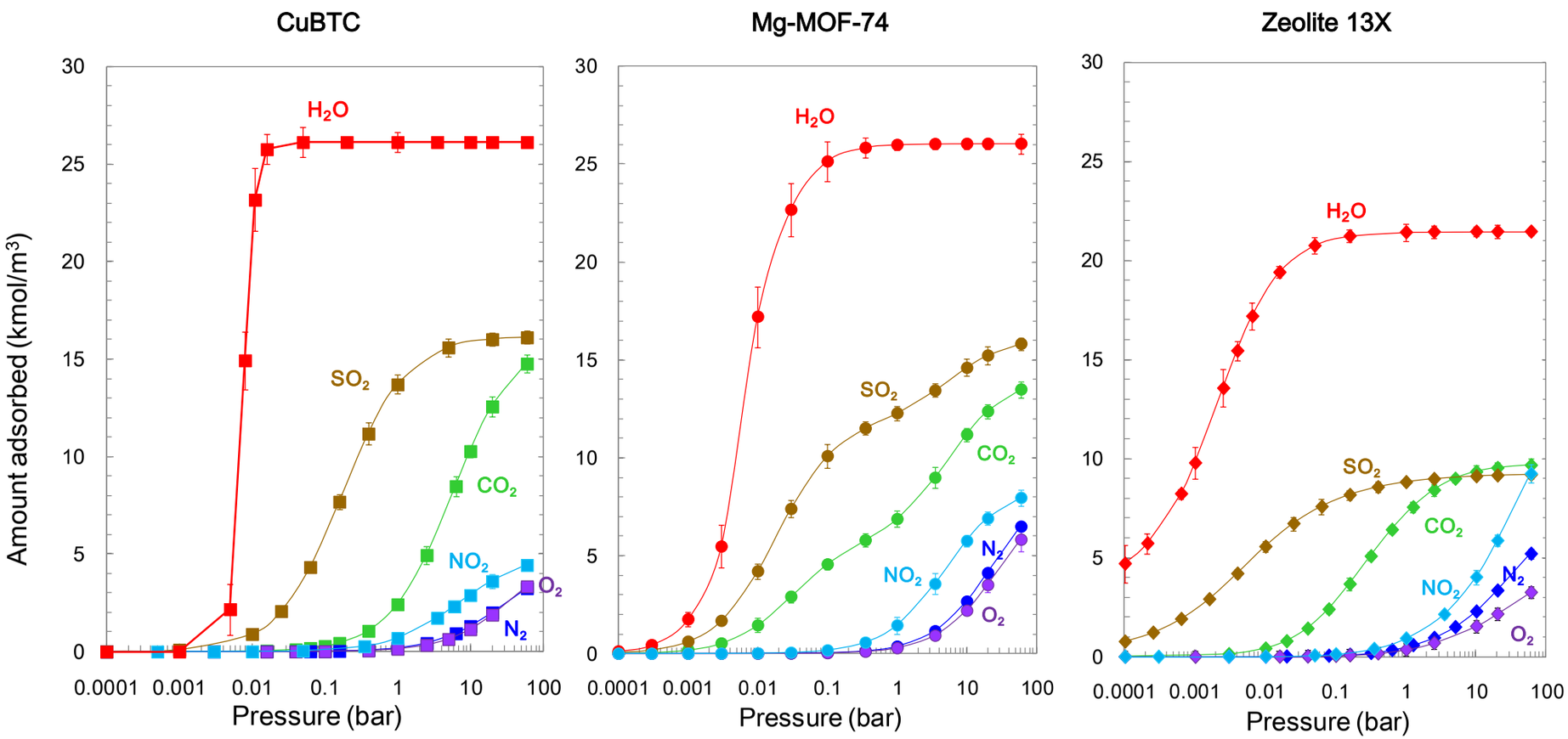

Figure 2. Comparison of simulated pure adsorption isotherms for CO_2, N_2, O_2, H_2O, SO_2 and NO_2 in the two selected MOFs and zeolite 13X at T=313K. Symbols represent GCMC results (squares, circles and diamonds for CuBTC, Mg-MOF-74 and zeolite 13X, respectively), and lines are guides to the eyes. The error bars represent the standard deviations.

3.2. CO_2/N_2 mixtures behavior without and with impurities

In an industrial post-combustion stream, in addition to nitrogen, CO_2 is accompanied by other compounds; hence, it is necessary to investigate the adsorption behavior in the presence of these contaminants for an accurate assessment of the performance of the material at process conditions. A typical composition for a post-combustion flue gas from coal-fired power plant contains 70–75% N_2, 15% CO_2, 3-4 % O_2, 5–7% water and traces of other species[106] (500 ppm NO_x and up to 2,000 ppm SO_2 when burning high-sulfur coals[107]). After previous impurity removal stages, the final temperature and pressure conditions are maintain close to 313-333 K and 1 bar, respectively, and some impurities remain as traces[108]. In this study, H_2O, SO_2 and NO_2 impurities concentrations were varied from a few tenths ppm up to 1%, keeping CO_2 in 15% and N_2 as the surplus. Since oxygen showed very similar behavior than nitrogen when adsorbed onto all three structures, O_2 was neglected for mixtures simulations.

Figure 3 shows CO_2 adsorption isotherms for CuBTC, Mg-MOF-74 and zeolite 13X, and their different behavior under several evaluated conditions: as pure component, for binary mixture and for 0.1% (*i.e.*, 1,000ppm) of impurity (H_2O, SO_2 and NO_2) in the stream. Since water shows the strongest affinity, 0.01% H_2O composition was also included.

As shown by some authors, the presence of unsaturated metal sites in CuBTC enhances the separation of CO_2 as water molecules coordinate with the metal clusters.[30,32] This behavior can be seen for the ternary mixture with 0.01% H_2O in the flue gas, where the adsorption isotherm of CO_2 in CuBTC shows an increase after a total water coordination at a pressure of 8bar (see Figure 3). Nevertheless, the induced enhanced selectivity results in competition sites between water and CO_2, and finally, with more

water molecules adsorbed at higher pressures (*e.g.* at 20bar), the competition leads to the decrease of the CO_2 adsorption capacity compared to the binary mixture. In addition, when CuBTC is exposed to 0.1% H_2O, its CO_2 adsorption capacity in mixtures significantly decreases. For instance, at 10bar the uptake reduction is about 55% (from 4.9 to 2.1 kmol/m^3).

A complete different behavior is observed for zeolite 13X: as H_2O molecules are pre-adsorbed in the pores, the CO_2 capacity decreases with the decrease of adsorption sites available on the porous surface. At 0.1% H_2O, the material becomes completely useless for CO_2 separation: water precludes any adsorption of CO_2 and N_2. Conversely, compositions of water in the stream affect the CO_2 uptake on Mg-MOF-74 in less extend than for CuBTC and 13X, being more notorious at higher pressures. For instance, for a mixture with 0.1% H_2O in the flue gas, a visible reduction in the isotherm is obtained for pressures above 2bar.

Regarding the other two impurities, SO_2 reduces the CO_2 capacity in 13X in greater manner than in the two MOFs structures, while the presence of NO_2 in the mixtures has almost no effect in the adsorption process: the maximum reduction for CO_2 uptake is seen in CuBTC, where the value decreases from 3.5 kmol/m^3 in the binary mixture to 3.3 kmol/m^3 in the presence of 0.1% of NO_2 at 10bar.

As above-mentioned, the isosteric heat of adsorption is an important property to be considered to assess the performance of the materials. For multiple molecules adsorbed at different sites of the structure, relatively different energy values will be obtained for each one, allowing a sampling assessment. Therefore, to identify adsorption features on the frameworks, distribution profiles of the isosteric heats were calculated at pure and mixture conditions for the different gas molecules.

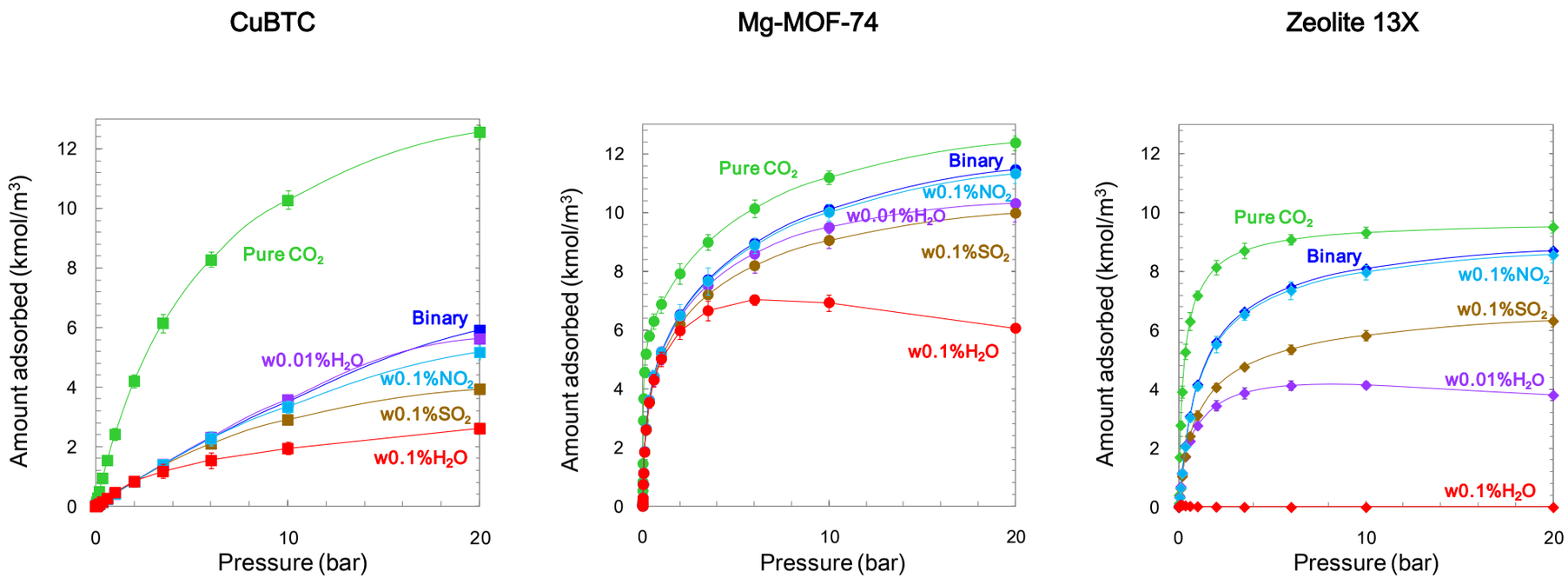

Figure 3. Comparison of simulated adsorption isotherms for pure carbon dioxide (in green) and the behavior under different mixture conditions: binary 15%CO_2/85%N_2 mixture (in dark blue), ternary 15%CO_2 /84.99%N_2 / 0.01%H_2O mixture (in purple), ternary 15%CO_2 / 84.9%N_2 / 0.1%H_2O mixture (in red), ternary 15%CO_2 / 84.9%N_2 / 0.1%SO_2 mixture (in brown) and ternary 15%CO_2 / 84.9%N_2 / 0.1%NO_2 mixture (in light blue). T =313K.

Figure 4 depicts the adsorption energy profiles for the different components studied in three ternary mixtures including impurities of H_2O, SO_2 and NO_2, respectively, compared to those in the pure state. Note that the mean value of each dotted histogram is the value presented in section 3.1. A displacement to lower energies with respect to the pure isotherm values is observed in most cases. For instance, the mixture behavior of carbon dioxide on CuBTC shows a higher peak related to the adsorption in the octahedral side pockets. Furthermore, it is important to notice that the mean adsorption energy obtained for carbon dioxide in CuBTC with mixture including 0.01%H_2O slightly shifts to higher energy values, reflecting the improved adsorption by the presence of water. Furthermore, SO_2 presents a radical change in energy distribution in CuBTC that can be explained by its competition with CO_2, being this MOF more attractive to the sulfur compound.

A shift in the maximum peak is also detected for N_2 in zeolite 13X. As two adsorption sites are differentiated for nitrogen in this material, this shift means a change in pore sizes where the molecule is adsorbing: N_2 prefers to be adsorbed in the interstices with intermediate diameter where it has greater interaction with the material. However, with the inclusion of competing species, nitrogen molecules tend to locate in the larger pores. Since CO_2 molecules are able to compete against water in a mixture with 0.01% H_2O in zeolite 13X, the CO_2 isosteric heat distribution is similar to the pure component, and water molecules are displaced to occupy lower energy sites. All these changes in isosteric heat will be taken into account for the calculation of energetic performances in the next section.

In addition to the results presented in this section, a comparison between the isosteric heat distributions of the molecules in all three materials for pure compounds and for the binary CO_2/N_2 mixture were also calculated and results are provided in Figure S9,

while selectivity for CO_2-over-N_2 for binary 85%N_2/15%CO_2 and ternary 15%CO_2/84.9%N_2/0.1%H_2O mixtures as function of pressure are shown in Figure S10 of the Supplementary Material. Results for the simulated adsorption isotherms of ternary mixtures at different conditions for the three materials can also be found in the Supplementary Material, Figures S11-S17.

3.3. Implications for the application in PSA, VSA and TSA processes.

Swing adsorption cycles can be manipulated to meet a variety of demanding requirements. For instance, same working capacities can be obtained by changing the adsorption/desorption conditions. Nevertheless, the most cost-effective material will lead the best selection for the CO_2 capture process.[85,109,110,111] The aim of this section is to test different conditions in order to be able to select, for each structure, those conditions that minimize the energy requirements for CO_2 capture. The chosen model has some idealized conditions that it is relevant to highlight: experimentally, there are changes in temperature during the adsorption/desorption steps, and also along the column. Besides, the maximum removal is achieved with no determined desorption time, and crystal activation of structures may not be always the same. These features are not considered in the simplified modeling used here hence, the results presented are for an ideal system, with higher purity and lower specific energy consumption values predicted than in the real case. However, the general trends obtained in this work should be maintained for practical implementations, as inferred from the agreement with parametric studies in the literature with similar adsorption/desorption conditions (see Figure S18 in the Supplementary Material).

Figure 5 summarizes different values for carbon dioxide working capacity in VSA, PSA and TSA processes, including all the mixtures evaluated in the previous section.

Six operating conditions are shown (two for each process), corresponding to 10bar→1bar and 20bar→1bar for PSA, 1bar→0.1bar and 1bar→0.05bar for VSA, while the TSA operating conditions under study were 383K→313K and 443K→313K. Constant condition of 313K was set for VSA and PSA, and pressure at 1bar for TSA.

For VSA conditions, zeolite 13X shows higher working capacities than CuBTC and Mg-MOF-74, especially when the pressure at the desorption step is lowered to 0.05 bar. However, when it comes to water traces in the mixture, MOFs structures show better performance. CO_2 working capacities decline after water sorption in almost all cases, being more noticeable in the zeolite, as already explained for the adsorption capacity.

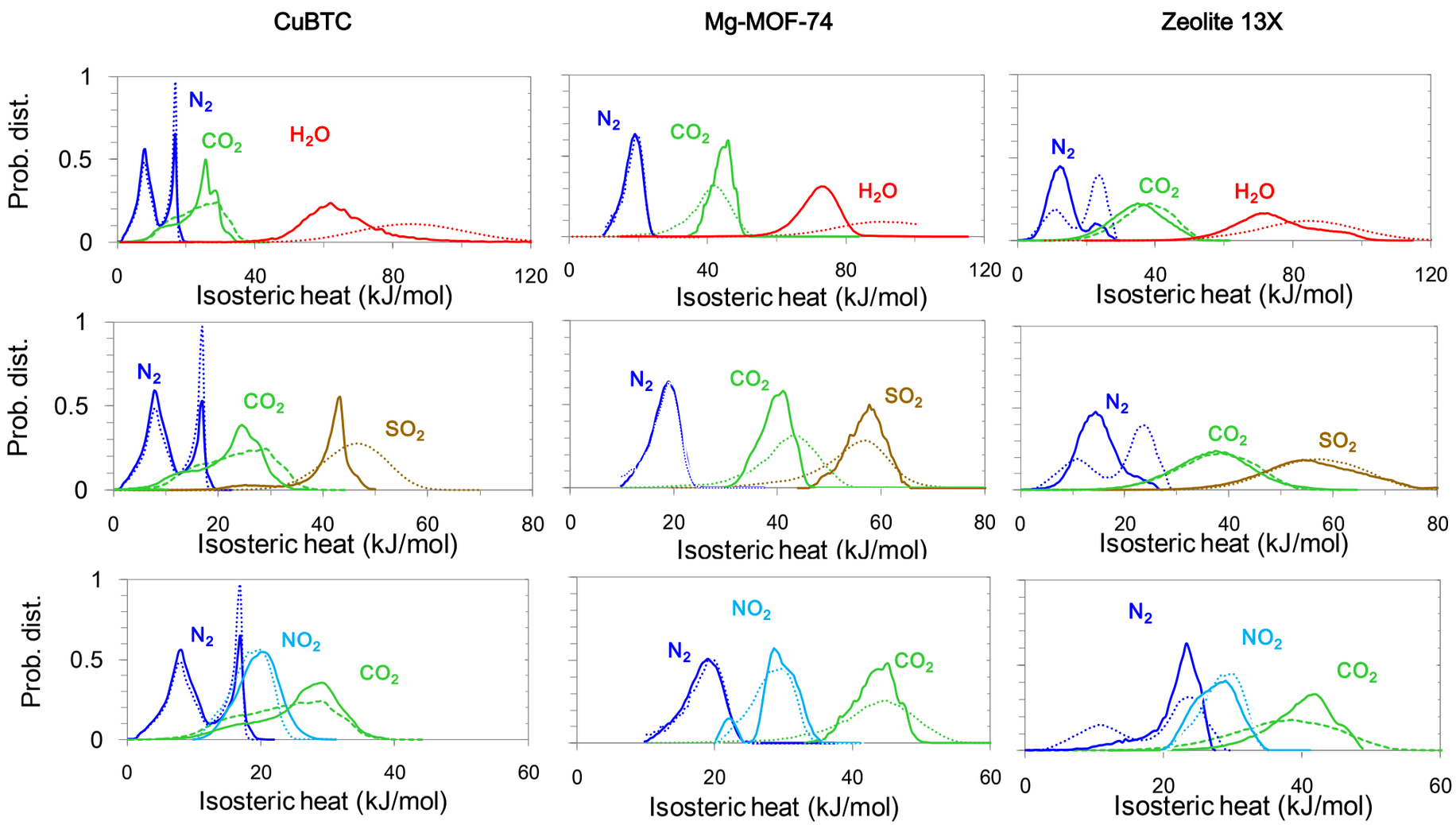
CuBTC
Mg-MOF-74
Zeolite 13X
Prob. dist.
Isosteric heat (kJ/mol)
N2
CO2
H2O
SO2
NO2

Figure 4. Isosteric heat distribution curves for pure (dotted line) and ternary mixtures (solid line) including 0.01%H_2O (top), 0.1%SO_2 (center) and 0.1%NO_2 (bottom) at a total pressure of 1bar and 313K, in CuBTC, Mg-MOF-74 and zeolite 13X.

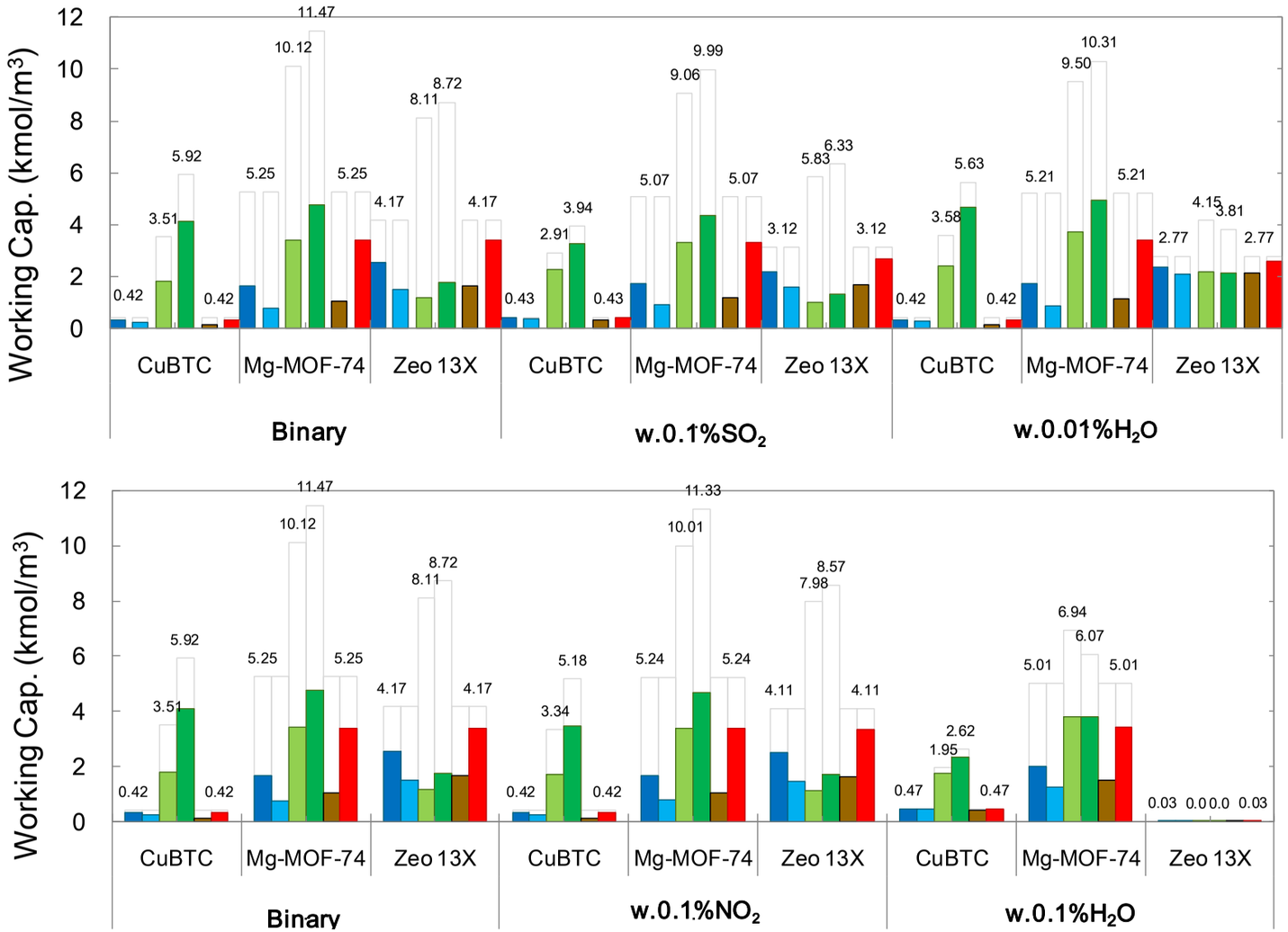

Figure 5. Calculated working capacities of CO_2 for swing adsorption processes at different flue gas conditions: a) binary 15%CO_2/85%N_2, b) ternary with sulfur dioxide, 15%CO_2/84.9%N_2/0.1%SO_2, c) ternary with water, 15%CO_2/84.99%N_2/0.01%H_2O, d) ternary with nitrogen dioxide, 15%CO_2/84.9%N_2/0.1%NO_2, and, e)

ternary 15%CO_2/84.9%N_2/0.1%H_2O. Greens, blues and reds columns represent PSA, VSA and TSA processes, respectively: light green for PSA 10bar→1bar, dark green for PSA 20bar→1bar, light blue for VSA 1bar→0.1bar, dark blue for VSA 1bar→0.05bar, brown for TSA 383K→313K and red for TSA 443K→313K. The uptake values at adsorption conditions of each one of the processes are shown as transparent columns above the working capacities.

It is worth mentioning that, while Mg-MOF-74 and zeolite 13X show high uptakes for VSA, the amount of CO_2 remaining in the adsorption bed at regenerating conditions is also high (*e.g.*, at 0.1bar, the remained amount of CO_2 in both structures is 3.7 and 2.9 kmol/m^3 respectively). Note also that desorption pressures below 0.10 bar are achievable in experiments,[112] while vacuum above 0.2-0.3bar can imply net values of working capacities of almost zero for Mg-MOF-74 and zeolite 13X (see Figure S19 in the Supplementary Material).

Moreover, working capacities in MOFs almost doubled the zeolite 13X behavior in all cases when the feeding pressure at adsorption conditions is raised from 10 to 20bar. For instance, CuBTC and Mg-MOF-74 present working capacities values in the binary mixture of 4.7 and 4.1 kmol/m^3, respectively (operating between 20→1 bar), compared to 1.7 kmol/m^3 for zeolite 13X. Moreover, Mg-MOF-74 offers the best results in PSA processes with impurities content, demonstrating that this material can be appropriate for this type of separation in spite of presenting slightly higher isosteric heats.

In some singular cases, see for instance, PSA 10→1bar with 0.1% SO_2 in CuBTC, and VSA 1→0.1bar with 0.01% H_2O in zeolite 13X, the working capacity value obtained is higher than the one from the binary mixtures. This is mainly due to a larger reduction in nitrogen than carbon dioxide adsorption capacity for competition with impurities.

CO_2 purity at the outlet of the adsorber is another important variable to consider, depending on the conditions required for its storage or different applications and the investment associated to it. Figures 6 and 7 show CO_2 purity (%) as a function of the recovery achieved (%). Each color line corresponds to a swing adsorption process

whether PSA, VSA or TSA, and the shape depends on the results obtained for a range of impurities up to 1% of SO_2, NO_2 and H_2O in the inlet flue gas (see also Figure 5).

It can be seen that recovery increases monotonically with purity in all three structures as the impurity content is increased, to a point where purity reaches its limit and shows a sharp drop in its value (or increase in some cases). The sudden change in that point is governed by the amount of carbon dioxide and the amount of nitrogen and impurities contained in the adsorption bed: a reduction in the CO_2 working capacity due to the uptake of competing components yields lower purities, while negligible N_2 working capacities allow higher purities.

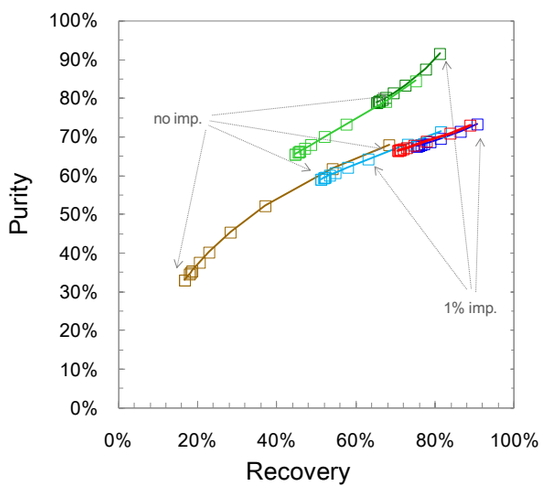

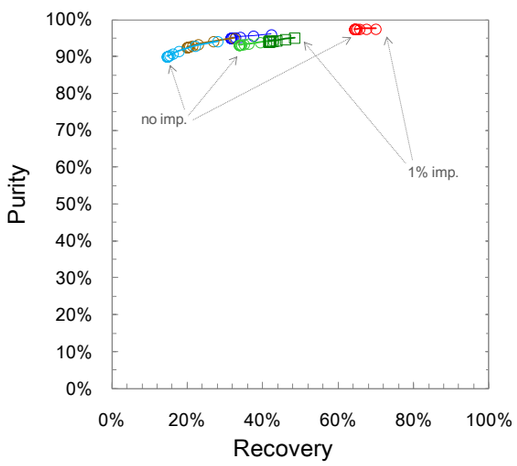

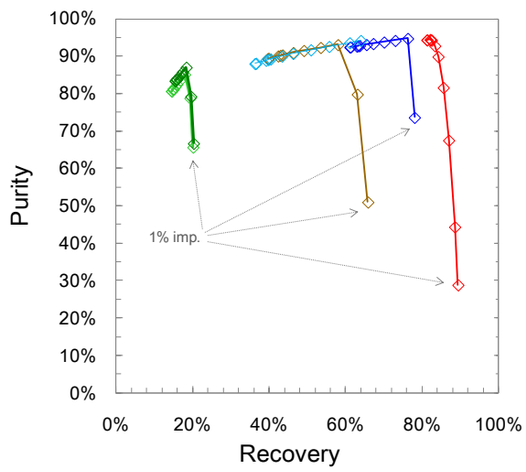

Figure 6. Curves of recovery evolution with purity for the evaluated swing adsorption processes, in the three studied adsorbents: CuBTC (top), Mg-MOF-74 (center) and zeolite 13X (bottom). Simulations performed at 313 K, assuming a packed bed with a void fraction of ϵ = 0.4 and SO_2 as impurity in a range from 10ppm (i.e., 0.001%) to 10,000ppm (i.e., 1%). Colors correspond to the processes mentioned in Figure 5.

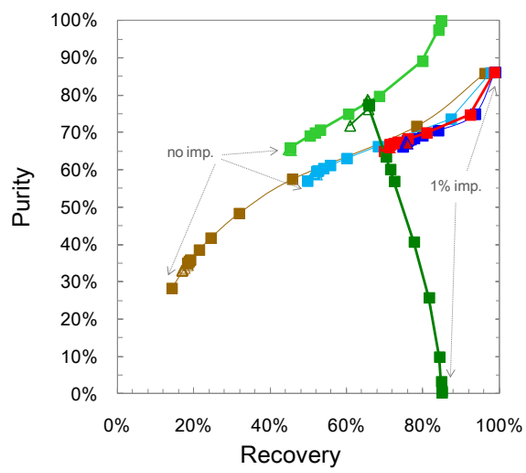

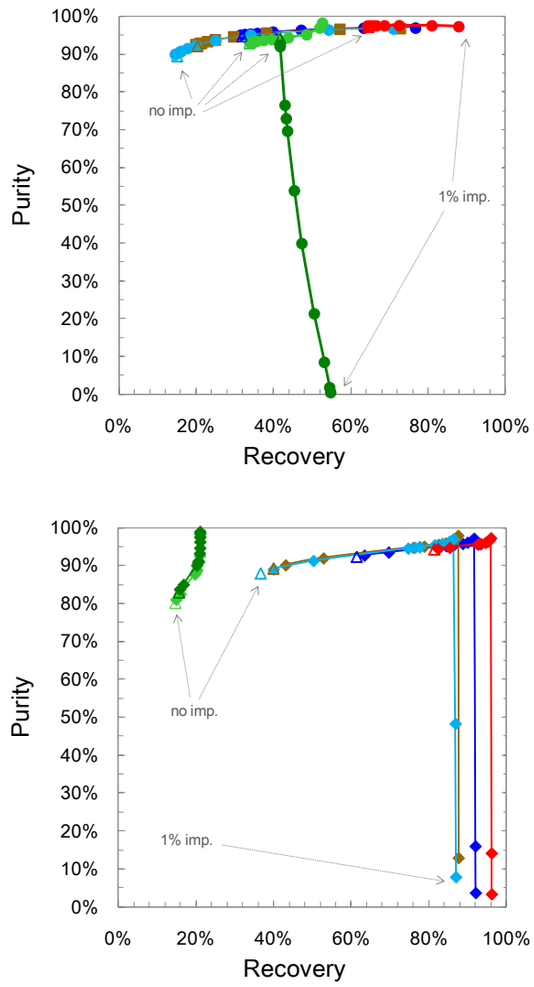

Figure 7. Curves of recovery evolution with purity for the evaluated swing adsorption processes, in the three studied adsorbents: CuBTC (top), Mg-MOF-74 (center) and zeolite 13X (bottom). Simulations performed at 313 K, assuming a packed bed with a void fraction of ϵ = 0.4 and water and NO_2 as impurities in a range from 10ppm (*i.e.,* 0.001%).to 10,000ppm (*i.e.,* 1%). Mixtures with H_2O in filled symbols and with NO_2 in open triangles. Colors correspond to the processes mentioned in Figure 5.

The increase in purity is not as substantial as the recovery for Mg-MOF-74 and zeolite 13X in the monotonically part of the curves. On the contrary, curves of CuBTC exhibit a more rounded shape and lower inflection points, as a consequence of its low CO_2-over-N_2 selectivity. To achieve CCS purity specifications for utilization, extreme desorption conditions would be needed for this material.

It can also be seen that VSA and TSA processes allow obtaining higher CO_2 purities than the PSA ones, because N_2 and impurities working capacities in PSA conditions are much higher and affect the composition at the outlet of the adsorber.

Surprisingly, impurities increase the curve inflection point, and the effect is more pronounced in mixtures with water than with SO_2 or NO_2, i.e., the higher the molecule affinity for all three materials and the difference with the isosteric heat of CO_2, the higher the inflection point that can be obtained in purity/recovery curves. In this study, the maximum inflection point is obtained for TSA at a desorbing temperature of 443K in all three materials, and with impurities compositions in the mixture of 1% H_2O for CuBTC, 0.5% H_2O for Mg-MOF-74 and 0.02% H_2O for zeolite 13X. For sulfur dioxide, the maximum point is achieved for mixtures including 1% SO_2, 1% SO_2, and 0.1% SO_2 for CuBTC, Mg-MOF-74 and zeolite 13X, respectively, but around 10-15% lower values in recovery are obtained.

Furthermore, since according to Figures 5 to 7, TSA allows recovering higher amounts of CO_2 than the other two processes, with higher purities, this process emerges as the most convenient so far. Nevertheless, the energy requirements for regeneration must be taken into consideration, as will be discussed in the next section.

3.3.1. Energetic requirements for the different processes

For fair comparison of energetic cost, PSA/VSA/TSA processes are compared for conditions with purities above 80% of CO_2. All three materials can reach this condition, according to the previous discussion, although only TSA and VSA processes can achieve recovery and purities above 90%, values commonly required for CCS specifications.[113] The additional fixed bed parameters used in swing adsorption processes simulations are provided in Table S2 in the Supplementary Material.

The higher the desorption temperature in TSA or the lower the desorption pressure in VSA, the higher the thermal energy or adiabatic work required. Decreasing the regeneration pressure in VSA processes from 0.1 to 0.05bar increases the adiabatic work per cycle by 30-40% approximately, but can be compensated with the extra amount of CO_2 recovered. In addition, desorption temperature significantly affects both the CO_2 working capacity and the thermal regeneration energy.[86] Consequently, there must be a tradeoff between energy costs and increased working capacities. Figures S19 to S21 (see Supplementary Material) show the variation of working capacity and energy required per cycle calculated by means of Eqs. (4) to (6), as a function of desorption condition.

The variation of purity, recovery and specific energy consumption with desorption pressure in VSA processes, adsorption pressure in PSA processes and desorption temperature in TSA processes are presented in Figures S22-24 in the Supplementary Material. Parameters implication on the process performance can be found elsewhere for mixtures without impurities and are omitted here.[39,84,109,110,112]

The evolution of the specific energy consumption (*i.e.*, the required energy per tonne of CO_2 captured and separated) with the increase of impurities percentage in the

mixture, is shown in Figure 8. The presence of H_2O, SO_2 and NO_2 as impurities with a percentage between 0.001% and 1% were considered, while the increase of the impurity is in detriment of the same N_2 percentage. Notice that, in order to compare TSA with pressure processes, an exergetic comparison was used, and further compression of the rich-CO_2 stream to supercritical fluid for transportation was not included in the calculations.

With these assumptions, TSA specific energy consumptions are the lowest in Mg-MOF-74 and zeolite 13X for impurities content lower than 0.5% and 0.02% respectively. Notice that although one of the best options for all three adsorbent materials is VSA with regeneration at 0.05bar, it is really difficult to expand in practice at so low pressure values, and therefore it may not be viable in certain plants.

As inferred from Figure 8, it is clear that zeolite 13X is more appropriate for VSA and TSA processes. However, the energy requirements increase as impurities are explicitly considered in the mixture, the change being sharper for impurities with higher isosteric heat, (*i.e.*, higher affinity); in this case, the increase in the slope follows the tendency $H_2O > SO_2 > NO_2$, (marked by the arrows in Figure 8). Although it was expected that H_2O and SO_2 carry out a negative influence in the total CO_2 recovery cost, at so low percentages, SO_2 does not exert a decisive influence in the process, since the quantity of adsorbed CO_2 is not drastically reduced below 0.1%.

It is remarkable that, in some cases, the addition of impurities reduces the energetic requirement per tonne of CO_2 captured. For instance, the requirements for VSA 1→0.1bar with Mg-MOF-74 shows a reduction from 4 GJ/tonne-CO_2 in the binary mixture to 2.7 GJ/tonne-CO_2 including 0.1% H_2O. SO_2 also shows this reduction, but is lesser than the one obtained for a more affinity species, while the minimum value is

achieved at a higher impurity concentration than water (shown by the arrows). The same behavior is observed for TSA processes in CuBTC.

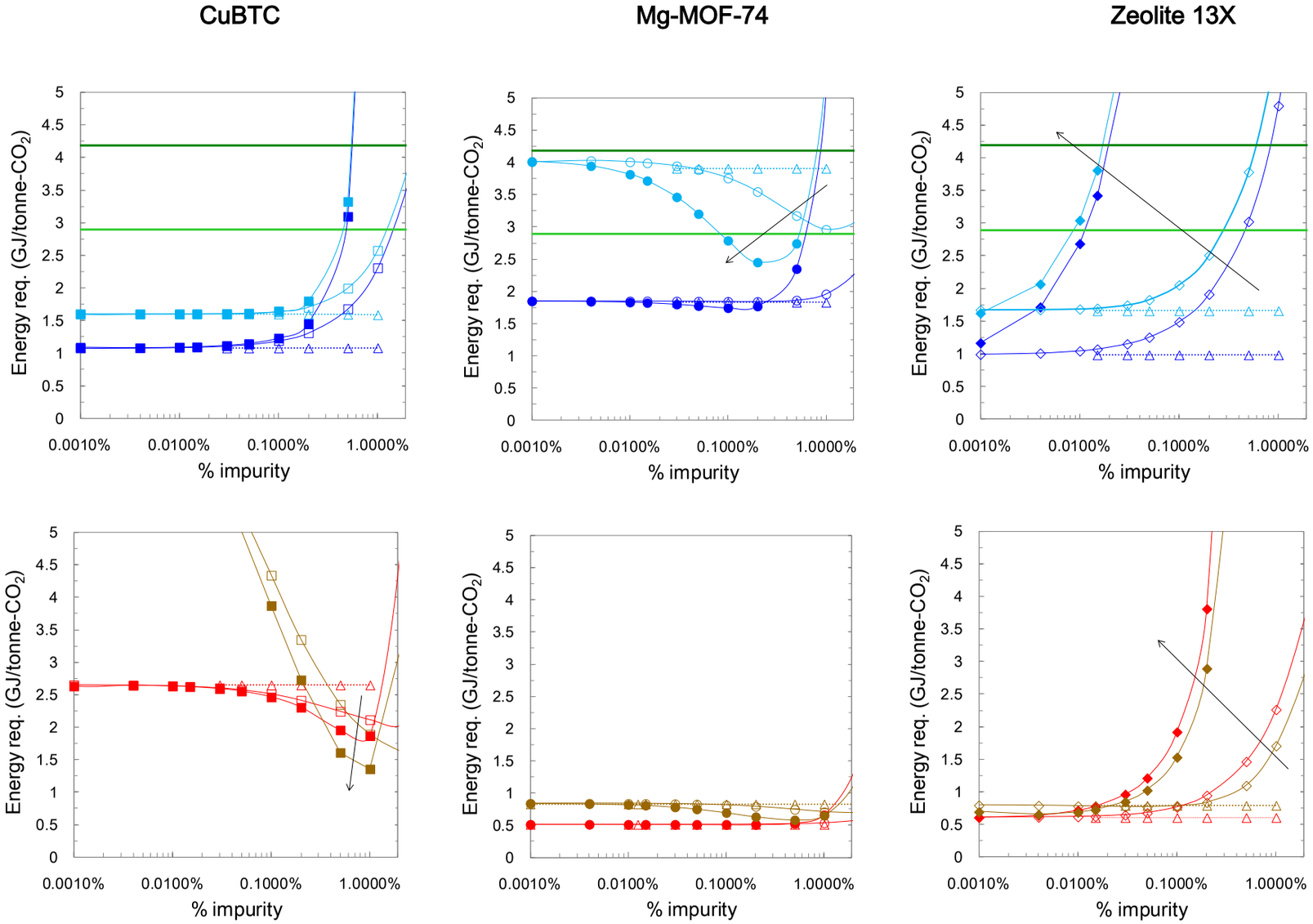
CuBTC
Mg-MOF-74
Zeolite 13X
Energy req. (GJ/tonne-CO2)
% impurity
0.0010%
0.0100%
0.1000%
1.0000%
0
0.5
1
1.5
2
2.5
3
3.5
4
4.5
5

Figure 8. Calculated energy quality (exergetic) requirements per tonne of CO_2 captured as impurity content function for swing adsorption processes: light green for PSA 10bar→1bar, dark green for PSA 20bar→1bar, light blue for VSA 1bar→0.1bar, dark blue for VSA 1bar→0.05bar, brown for TSA 383K→313K and red for TSA 443K→313K. Filled symbols for water, open symbols for sulfur dioxide and dotted lines with triangles for nitrogen dioxide. Arrows indicate the trend as the isosteric heat of the impurity is higher.

In addition, GJ/tonne-CO_2 values obtained with NO_2 as impurity show almost constant specific consumption energy within this concentration range.

Even though MOFs are more appropriate than zeolite 13X for PSA systems due to a higher CO_2 uptake, the obtained purity and recovery values are lower and the energy requirements are the highest of the three technologies evaluated. In this case, their values are basically constant over the entire concentration range since it does not depends on the working capacity of other species besides CO_2, due to the "no purge" assumption. Nevertheless, impurity content above 1% in all three materials makes this technology competitive.

The minimal energy consumption and the maxima productivity (understood in this context as working capacity) do not coincide, in general, in the same operating point. Instead, there exists a so-called frontier zone where local minimum and maximum can be obtained for these two parameters. Multiple swing adsorption devices can be coupled with slightly beneficial effect on the purity of the recovered product.[114,115] However, this comes at the expense of recovery and an increase in power requirement (energy penalty). An analysis of these effects lies out of the scope of this study.

3.3.2. Combined swing adsorption cycles

TSA is a particularly promising process for post-combustion CO_2 capture, owing to difficulties with compressing or applying a vacuum to large volumes of flue gas streams.[24,116,117] It is a very versatile process in terms of cycle design and ability to adapt to changes in feed gas conditions (recovery, purity, energy consumption). However, the longer time required for extreme heating/cooling (and therefore productivity) may limit its application for CO_2 capture at large scale. Dynamic/kinetic performance is out of the

scope of this study, but just to mention that the cycle time will increase with increasing the desorption temperature, and hence, the productivity obtained will be lower. The same is expected for extreme pressurization and/or evacuation conditions.

Convenient procedures for CO_2 adsorption could be processes in which the adsorption step takes place at moderate pressures above atmospheric conditions, where expensive compression units are not required, and desorption is performed also under moderate vacuum conditions or a small heating of the system.[118,119] These hybrid processes are called VPSA, PTSA and VTSA, according to the combine techniques, and are even more attractive for their commercial implementation because of the low energy demand. Recently, some researchers have studied the use these hybrid processes to improve the CO_2 capture.[45,116,120,121]

A detailed study of the energy consumption of these hybrid processes has been also performed for the materials investigated in this work. Figure 9 shows a comparison of contour maps of specific energy quality consumption for VTSA processes, as a function of the desorption conditions T_{regen} (in the *x*-axe) and P_{regen} (in the *y*-axe). VPSA and PTSA processes are not included in the main body of the manuscript because they achieve lower purities and recoveries than those required for CCS specification and higher specific energy consumptions. Results including parameters such as specific energy requirements, working capacity, purity and recovery of these hybrid cycles can be found in Figures S25-S27 of the Supplementary Material.

The exergetic parameters of CuBTC, Mg-MOF-74 and 13X are compared without impurity content and for three different conditions with impurities in VTSA processes; the impurities content where chosen from Figure 8 in the range showing lower specific energy consumption presented in section 3.3.1, but maintaining a

reasonable purity and working capacity. According to this, the evaluated conditions were: 0.1% H_2O and 0.1% SO_2 in CuBTC, 0.1% H_2O and 0.1% SO_2 in Mg-MOF-74, and 0.01% H_2O and 0.01% SO_2 in zeolite 13X.

As expected, higher working capacities and higher specific energy consumptions are achieved for operating conditions presenting a large cyclic capacity,[117] however, as mentioned before, a tradeoff must be achieved between these two parameters. Hence, highlighted squares in each contour map depict the hot spot regions where high working capacities can be obtained, purities and recoveries above 80-90%, and without incurring in extremely high energetic requirements. It is also interesting to note the change in shape of the contour maps when impurities are considered. Moreover, the minimum obtained in most cases improves the binary performance by increasing the purity and recovery achieved.

Specific energy (*i.e.*, exergy) consumption close to 1 GJ/tonne-CO_2 that maximizes working capacities and purities in all three structures were found. For CuBTC, a proposed condition is to desorb at 0.15bar, 343K, and with 0.1% SO_2. With a working capacity of 0.38 kmol/m^3, specific energy consumption of 1.21 GJ/tonne-CO_2, 81% purity and 92% recovery, this condition enhances the working capacity by 40%, and purity in more than 30%, with an increase in only 15% on the energy required, compared to the same conditions in the binary mixture.

For Mg-MOF-74, an attractive point is to desorb at 0.2bar and 423K, obtaining a working capacity of 3.5kmol/m^3, specific energy consumption of 0.36 GJ/tonne-CO_2, 98% purity and 86% recovery for binary mixture.

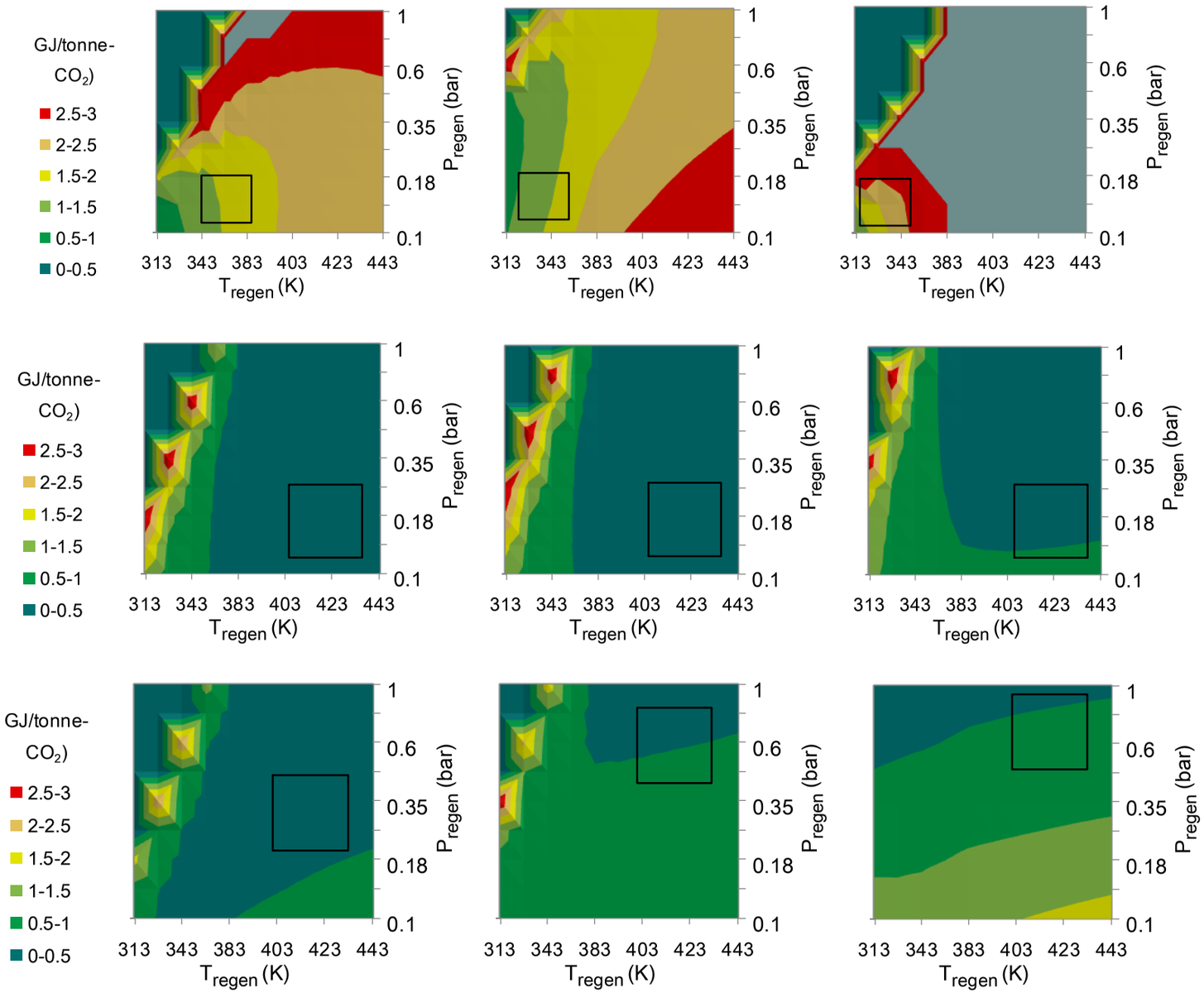
GJ/tonne-CO2)
2.5-3
2-2.5
1.5-2
1-1.5
0.5-1
0-0.5
1
0.6
0.35
0.18
0.1
Pregen (bar)
313 343 383 403 423 443
Tregen (K)

Figure 9. Contour maps of energy required per tonne of CO_2 captured as a function of desorption pressure and temperature conditions in VTSA processes: CuBTC (top), Mg-MOF-74 (center) and zeolite 13X (bottom). Comparison between binary mixture (left), ternary mixture with SO_2 traces (center) and ternary mixture with H_2O traces (right).

In this case, the inclusion of traces when adsorbing in Mg-MOF-74 reduces all parameters, and therefore the recovery is not encouraging. Lastly, for zeolite 13X, the selected point is to desorb at 0.6bar, 413K, and with SO_2 traces. The working capacity, specific energy consumption, purity and recovery obtained are 2.5 kmol/m^3, 0.46 GJ/tonne-CO_2, 92% and 82% respectively, with changes in -19%, +17%, +10% and +4% in all four parameters.

To compare this "optima" conditions with the ones obtained for regular PSA/VSA/TSA processes in the previous section, Figure 10 shows the performance of the best conditions in terms of specific energy consumption (*i.e.*, exergy) and working capacity for the processes achieving CCS specifications. The diameter of the bubble is referred to the purity obtained. It can be seen that higher working capacities with lower energy consumptions are achievable with Mg-MOF-74, while the energy consumption can be lowered by more than 30% with respect to zeolite 13X (and up to 10% including impurities).

In addition, the efficiency of the processes were calculated according to Zhao *et al.*:[111,122] the minimum work was obtained by calculating the mixture entropies and the composition that showed the best performance in each material (flue gas conditions: T=313K, P=1bar). Values obtained are as high as 35-40%, obtained specifically for the improved VTSA processes, and even higher than the typical values reported in the literature[112] (*i.e.*, between 10 and 30%).

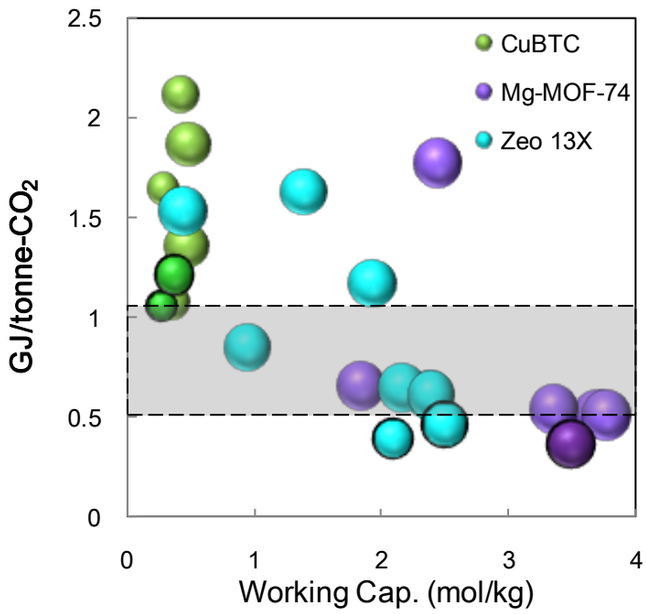

Figure 10. Specific energy consumption vs. CO_2 recovered for selected swing adsorption processes showing the better performance in each material. VTSA processes shown as highlighted bubbles. For comparison, energetic performance range for amines are in the range between the dotted lines (marked in grey).

In addition to 13X, the selected processes were compared with absorption processes based on the heat duty of the stripper: for the classical monoethanolamine (MEA) solvent,[4,123] the exergetic requirement of the process is between 0.9–1.0 GJ/tonne-CO_2. Value as low as 0.5 GJ/tonne-CO_2 can be achieved by industrial pilot tests based on DMX process[124], or with a mixture of amines as solvent.[125] The minimal value obtained in this work is similar to these values, in the range of the one obtained by Chaffe *et al*.[83] with VSA, but with higher purities and recoveries, and, in addition, significantly lower (almost 50%) than a reported 6-step TSA cycle[117] and a PVSA[110,114] based on zeolite. Adsorption processes are, however, close but not as mature as absorption processes yet for large scale CCS. Nevertheless, this study reinforces the

need to explore impurities species that can reduce the energy consumption, but increase the working capacity, purity and recovery only by modifying the trace composition as a step forward so that these technologies are competitive for CO_2 capture at large scale.

4. CONCLUSIONS

Molecular simulations and macroscopic thermodynamics were combined in this work to develop a model to account for the effect of impurities on two MOFs, CuBTC and Mg-MOF-74, on the performance of PSA, VSA and TSA processes, compared with zeolite 13X. The materials were chosen based on promising results from the literature regarding their performance for CO_2 capture and separation and also because they are already available in the market, while detailed studies regarding their implementation at process conditions were still missing. Adsorption and separation behavior towards carbon dioxide from nitrogen, with and without including impurities such as water, SO_2 and NO_2, were evaluated in this work. The first part of the study was carried out using GCMC simulations for the purpose of identifying key structural properties for selective adsorption from a post combustion stream. The force fields used for the simulations were validated versus available experimental data for pure components and used in a predictive manner for multicomponent study. The ability of the adsorbent materials was checked by comparing mixture isotherms and isosteric heats, while the evaluation for potential material for purification was comprehensively examined by working capacities and energy performance in the mentioned swing adsorption processes. Hot spot regions for each process and materials were identified considering where high working capacities can be obtained, purities and recoveries above 80-90%, and without incurring in extremely high energetic requirements.

Results reveal that zeolite 13X become useless with less than 0.1% of water content in the mixture, and just a 0.01% of moisture in the adsorbent is able to significantly reduce the CO_2 adsorption capacity. Conversely, it was found that even with a concentration of SO_2 and NO_2 in the flue gas as high as 1,000ppm (*i.e.*, 0.1%), the energy performance (GJ/tonne-CO_2) in the flue gas mixtures remains essentially unaffected. In addition, purity and recovery can be highly increased with slightly lower working capacities, attributed to the introduction of a certain amount of competitive molecules in the flue gas. Moreover, these impurities traces can be beneficial and reduce the exergetic requirements per tonne of CO_2 captured up to a certain inflection value where the increase in energy cost becomes exponential. The minimum energy requirement inflection points were obtained for TSA at a desorbing temperature of 443K in all three materials, and with impurities compositions in the mixture of 1% H_2O for CuBTC, 0.5% H_2O for Mg-MOF-74 and 0.02% H_2O for zeolite 13X (with values of 1.13, 0.55 and 0.58 GJ/tCO_2, respectively).

After considering operating conditions and with respect to the results presented here, Mg-MOF-74 stands up as one of the most promising materials to be used in TSA/VTSA processes for its great performance and “buffer” behavior with the inclusion of lower amounts of impurities. Moreover, CuBTC emerges as a good candidate for separation when higher moisture or impurity content above 1% is present in the mixture, and purity is not a determinant factor.

This study represents a first quantitative assessment of the process performance that can be achieved including impurities effects onto novel adsorbent materials in VSA/PSA/TSA process for CO_2 capture. Further studies will include detailed modeling

by solving the differential equations describing the different steps of the adsorption processes, to account for time-dependent phenomena inside the adsorption beds.

NOMENCLATURE

BTC Benzene-1,3,5-tricarboxylate

C_P heat capacity of the adsorbent material [kJ/kg-K]

DOBDC 2,5-dioxido-1,4-benzenedicarboxylate

E total energy of the system [kJ]

E_{ij} potential energy between a pair of atoms i and j [kJ/mol]

GCMC Grand canonical Monte Carlo

IAST Ideal Adsorption Solution Theory

LJ Lennard-Jones

MOF Metal organic framework

$\mathcal{N}$ adsorbed molecules (mol)

n amount adsorbed per mass [mol/kg] or per volume [kmol/m^3] of adsorbent

P pressure [bar]

PSA Pressure swing adsorption

$Q_{thermal}$ energy requirement for heat [kJ]

q_i partial charge of atom i

q_{ST} isosteric heat of adsorption [kJ/mol]

R gas constant [8.314 kJ/mol-K)

r_{ij} distance between a pair of atoms i and j [Å]

T temperature [K]

TSA Temperature Swing Adsorption

V total volume of packed bed [m^3]

VSA Vacuum Swing Adsorption

W adiabatic energy requirement for compression/vacuum [kJ]

x mole fraction of component *k* in the adsorbed phase

y mole fraction of component *k* in the gas phase

Greek symbols:

Δn working capacity [mol/kg]

ϵ voidage of bed

ε_{ij} Lennard-Jones potential well depth [kJ/mol]

ε_0 vacuum permittivity [F/m]

γ polytropic parameter of gases

η feeding/vacuum blower efficiency

ρ_S framework density [kg/m^3]

σ_{ij} Lennard-Jones potential diameter [Å]

θ total number of moles where compression or vacuum is effectuated [mol]

μ chemical potential [kJ/mol]

Suscripts:

$ads/feed$ adsorption or feeding conditions

$des/regen$ desorption or regeneration conditions

k species in the gas mixture *($k = CO_2, N_2, H_2O, \ldots$)*

APPENDIX A. Supplementary Material

Figures of the different pore sizes in CuBTC, Mg-MOF-74 and zeolite 13X frameworks, molecular parameter values for the force fields, comparison of calculated pure adsorption isotherms with experimental data, isosteric heat distribution profiles for pure components and their changes with coverage, as well as adsorption isotherms behavior for binary (CO_2/N_2 at different conditions), and ternary ($CO_2/N_2/H_2O$, $CO_2/N_2/SO_2$ and $CO_2/N_2/NO_2$) streams for the three materials. In addition, profiles with energetic performance including energy requirements behavior under different desorbing conditions for swing adsorption processes, as well as combined VPSA, PTSA and VTSA processes.

This data, associated with this article, can be found in the online version.

ACKNOWLEDGMENT

We acknowledge helpful discussions with Hermenegildo Garcia, Concha Domingo and Francisco Medina during the early development of this work. Financial support from the Spanish government under project CTQ2014-53987-R and the Generalitat of Catalonia under project 2014SGR1582 is gratefully acknowledged.

NOTES

The authors declare no competing financial interest.

REFERENCES

[1] International Energy Agency (IEA). *CO_2 Capture and Storage: A key carbon abatement option*. *Energy Technology Analysis*. **2008**. ISBN 978-92-64-04140-0.

[2] Leung, D. Y. C.; Caramanna, G.; Maroto-Valer, M. M. An overview of current status of carbon dioxide capture and storage technologies. *Renewable and Sustainable Energy Reviews*, **2014**, *39*: 426-443.

[3] Kohl, A.; Nielsen, R. *Gas Purification*, fifth edition, Gulf Publishing Co., Houston, TX, **1997**. ISBN-10: 0884152200.

[4] International Energy Agency (IEA). Improvement in Power Generation with Post-Combustion Capture of CO_2, Report No. PH4/33, **2004**.

[5] Rochelle, G. T. Amine scrubbing for CO_2 capture. *Science* **2009**, *325*: 1652–1654.

[6] Yu, C.-H.; Huang, C.-H.; Tan, C.-S. A Review of CO_2 Capture by Absorption and Adsorption. *Aerosol Air Qual*. *Res*., **2012**, *12*: 745–769.

[7] Sumida, K.; Rogow, D. L.; Mason, J. A.; McDonald, T. M.; Bloch, E. D.; Herm, Z. R.; Bae, T.-H.; Long, J. R. Carbon Dioxide Capture in Metal–Organic Frameworks. *Chem*. *Rev*. **2012**, *112*: 724–781.

[8] Sayari, A., Belmabkhout, Y.; Serna-Guerrero, R. Flue gas treatment via CO_2 adsorption. *Chem*. *Eng*. *J*. **2011,** *171*: 760–774.

[9] Cavenati, S.; Grande C. A.; Rodrigues A. E. J. Adsorption Equilibrium of Methane, Carbon Dioxide, and Nitrogen on Zeolite 13X at High Pressures. *Chem*. *Eng*. *Data*. **2004**, *49*: 1095-1101.

[10] Li, J.-R., Ma, Y., McCarthy, M. C., Sculley, J., Yu, J., Jeong, H.-K., Balbuena, P. B., Zhou, H.-C. Carbon dioxide capture-related gas adsorption and separation in metal-organic frameworks. *Coord*. *Chem*.. **2011**, *255*: 1791-1823.

[11] Yaghi, Ö. M.; O'Keeffe, M.; Ockwig, N.W.; Chae, H.K.; Eddaoudi, M.; Kim, J. Reticular synthesis and the design of new materials. *Nature*. **2003**, *423*: 705-714.

[12] Rowsell, J. L. C.; Yaghi, Ö.M. Metal–organic frameworks: a new class of porous materials. *Microporous Mesoporous Mater*. **2004**, 73: 3-14.

[13] Kitagawa, S.; Kitaura, R.; Noro, S. Functional Porous Coordination Polymers. *Angew*. *Chem Int*. *Ed*. **2004**, *43*: 2334-2375.

[14] Snurr, R. Q.; Hupp, J. T.; Nguyen, S. T. Prospects for nanoporous metal-organic materials in advanced separations processes. *AIChE J*. **2004**, *50*: 1090-1095.

[15] Ferey, G. Hybrid porous solids: past, present, future. *Chem*. *Soc*. *Rev*. **2008**, *37*: 191-214.

[16] Eddaoudi, M; Kim, J; Rosi, N; Vodak, D; Wachter, J; O'Keeffe, M; Yaghi, Ö. M. Systematic Design of Pore Size and Functionality in Isoreticular MOFs and Their Application in Methane Storage. *Science*. **2002**, *295*(5554): 469-472.

[17] Karra, J. R.; Walton, K. S. Effect of Open Metal Sites on Adsorption of Polar and Nonpolar Molecules in Metal−Organic Framework Cu-BTC. *Langmuir*. **2008**, *24*: 8620-8626.

[18] Wang, Q.; Shen, D.; Buelow, M.; Lau, M.; Deng, S.; Fitch, F. R.; Lemcoff N. O.; Semanscin, J. Metallo-organic molecular sieve for gas separation and purification. *Microporous Mesoporous Mater*. **2002**, *55*: 217-230.

[19] Xiang, S.; He, Y.; Zhang, Z.; Wu, H.; Zhou, W.; Krishna, R.; Chen, B. Microporous metal-organic framework with potential for carbon dioxide capture at ambient conditions, *Nature Comm*. **2012**, *3*: 954.

[20] Bourrelly, S.; Llewellyn, P. L.; Serre, C.; Millange, F.; Loisean, T.; Ferey, G. Different Adsorption Behaviors of Methane and Carbon Dioxide in the Isotypic Nanoporous Metal Terephthalates MIL-53 and MIL-47. *J*. *Am*. *Chem*. *Soc*. **2005**, *127*: 13519-13521.

[21] Chui, S. S. Y.; Lo, S. M. F.; Charmant, J. P. H.; Orpen, A. G.; Williams, I. D. A chemically functionalizable nanoporous material. *Science*. **1999**, *283*(5405): 1148-1150.

[22] Millward, A. R.; Yaghi, Ö. M. Metal−Organic Frameworks with Exceptionally High Capacity for Storage of Carbon Dioxide at Room Temperature. *J*. *Am*. *Chem*. *Soc*. **2005**, *127*(51): 17998-17999.

[23] Yang, Y.; Shukla, P.; Wang, S.; Rudolph, V.; Chen, X.-M.; Zhu, Z. Significant improvement of surface area and CO_2 adsorption of Cu–BTC via solvent exchange activation. *RSC Adv*. **2013**, *3*: 17065-17072.

[24] Mason, J. A., Sumida, K., Herm, Z. R., Krishna, R., Long, J. R. Evaluating metal–organic frameworks for post-combustion carbon dioxide capture via temperature swing adsorption. *Energy Environ*. *Sci*. **2011**, *4*: 3030–3040.

[25] Yu, J., Balbuena, P. B. Water Effects on Postcombustion CO_2 Capture in Mg-MOF-74. *J*. *Phys*. *Chem*. *C*. **2013**, *117*: 3383–3388.

[26] Valenzano, L.; Civalleri, B.; Chavan, S.; Palomino, G. T.; Areán, C. O.; Bordiga, S. Computational and Experimental Studies on the Adsorption of CO, N_2, and CO_2 on Mg-MOF-74. *J*. *Phys*. *Chem*., **2010**, *114*: 11185-11191.

[27] Krishna, R.; Long, J. R. Screening Metal–Organic Frameworks by Analysis of Transient Breakthrough of Gas Mixtures in a Fixed Bed Adsorber. *J*. *Phys*. *Chem*. *C*. **2011**, *115*: 12941–12950.

[28] Liu, J.; Wang, Y.; Benin, A. I.; Jakubczak, P.; Willis, R. R.; LeVan, M. D. CO_2/H_2O Adsorption Equilibrium and Rates on Metal−Organic Frameworks: HKUST-1 and Ni/DOBDC. *Langmuir*. **2010**, *26*: 14301-14307.

[29] Talu, O. Measurements and analysis of mixture adsorption equilibrium in porous solids, *Chem*. *Ing*. *Technol*. **2011**, *83*: 67-82.

[30] Yazaydin, A. Ö.; Benin, A. I.; Faheem, S. A.; Jakubczak, P.; Low, J. J.; Willis, R. R.; Snurr, R. Q. Enhanced CO_2 Adsorption in Metal-Organic Frameworks via Occupation of Open-Metal Sites by Coordinated Water Molecules. *Chem*. *Mater*. **2009**, *21*(8): 1425-1430.

[31] Yu, K.; Kiesling, K: Schmidt. J. R. Trace Flue Gas Contaminants Poison Coordinatively Unsaturated Metal–Organic Frameworks: Implications for CO_2 Adsorption and Separation. *J*. *Phys*. *Chem*. *C*. **2012**, *116*: 20480−20488.

[32] Supronowicz, B.; Mavrandonakis, A.; Heine, T. Interaction of Small Gases with the Unsaturated Metal Centers of the HKUST-1 Metal Organic Framework. *J*. *Phys*. *Chem*. *C*. **2013**, *117*: 14570−14578.

[33] Castillo, J. M.; Vlugt, T. H. J.; Calero, S. *J*. Understanding Water Adsorption in Cu−BTC Metal−Organic Frameworks. *Phys*. *Chem*. *C*. *Lett*. **2008**, *112*(41): 15934-15939.

[34] Tan, K.; Zuluaga S.; Wang, H.; Canepa, P.; Soliman, K.; Cure, J.; Li, J.; Thonhauser, T.; Chabal, Y. J. Interaction of Acid Gases SO_2 and NO_2 with Coordinatively Unsaturated Metal Organic Frameworks: M- MOF-74 (M = Zn, Mg, Ni, Co). *Chem*. *Mater*., **2017**, *29*: 4227−4235.

[35] Liu, Y.; Liu, J.; Lin, J. Y. S.; Chang, M. Effects of water vapor and trace gas impurities in flue gas on CO_2/N_2 separation using ZIF-68. *J*. *Phys*. *Chem*. *C*., **2014**, *118*(13), 6744–6751.

[36] Yu, J.; Ma, Y.; Balbuena. P. B. Evaluation of the Impact of H_2O, O_2, and SO_2 on Postcombustion CO_2 Capture in Metal–Organic Frameworks. *Langmuir*. **2012**, *28*: 8064−8071.

[37] Ding, L.; Yazaydin, A. O. How Well Do Metal–Organic Frameworks Tolerate Flue Gas Impurities?. *J*. *Phys*. *Chem*. *C*. **2012**, *116*: 22987−22991.

[38] Glover, T. G.; Peterson, G. W.; Schindler, B. J.; Britt, D.; Yaghi, O. MOF-74 building unit has a direct impact on toxic gas adsorption. *Chem*. *Eng*. *Sci*., **2011**, *66*: 163-170.

[39] Li, G.; Xiao, P.; Webley, P.; Zhang, J.; Singh, R.; Marshall, M. Capture of CO_2 from high humidity flue gas by vacuum swing adsorption with zeolite 13X. *Adsorption*, **2008**, *14*(2): 415-422.

[40] Li, G.; Xiao, P.; Zhang, J.; Webley, P.; Xu, D. The Role of Water on Postcombustion CO_2 Capture by Vacuum Swing Adsorption: Bed Layering and Purge to Feed Ratio. *AIChE J*., **2014**, *60*(2): 673-689.

[41] Yu, J.; Wu, Y.; Balbuena, P. B. Response of Metal Sites toward Water Effects on Postcombustion CO_2 Capture in Metal−Organic Frameworks. *ACS Sustainable Chem*. *Eng*. **2016**, *4*: 2387−2394.

[42] Lee, K.; Howe, J. D.; Lin, L-Ch; Smit, B.; Neaton, J. B. Small-Molecule Adsorption in Open-Site Metal–Organic Frameworks: A Systematic Density Functional Theory Study for Rational Design. *Chem*. *Mater*. **2015**, *27*: 668−678.

[43] Xie, J.; Yan, N.; Yang, S. Synthesis, characterization and experimental investigation of Cu-BTC as CO_2 adsorbent from flue gas. *J*. *Environ*. *Sci*. **2012**, *24*(4): 640–644.

[44] Sun, W.; Lin, L.-C.; Peng, X., Smit, B. Computational screening of porous metal-organic frameworks and zeolites for the removal of SO_2 and NOx from flue gases. *AIChE J*. **2014**, *60*: 2314-2323.

[45] Liu, Q.; Ning, L.; Zheng, S.; Tao, M.; Shi, Y.; He, Y. Adsorption of Carbon Dioxide by MIL-101(Cr): Regeneration Conditions and Influence of Flue Gas Contaminants. *Nature, Scientific Reports*. **2013**, *3*: 2916.

[46] Meek, S. T.; Greathouse, J. A.; Allendorf, M. D. Metal-Organic Frameworks: A Rapidly Growing Class of Versatile Nanoporous Materials. *Advanced Materials*, **2011**, *23*: 249-267.

[47] Smit, B.; Maesen, T. L. M. Molecular simulations of zeolites: adsorption, diffusion, and shape selectivity. *Chem. Rev.*, **2008**, *108*: 4125-4184.

[48] Bahamon, D.; Vega, L. F.; Systematic evaluation of materials for post-combustion CO_2 capture in a Temperature Swing Adsorption process. *Chem. Eng. J.*, **2016**, *284*: 438–447.

[49] Goeppert, A.; Czaun, M.; Prakash, G. K. S.; Olah, G. A. Air as the renewable carbon source of the future: an overview of CO_2 capture from the atmosphere. *Energy Environ. Sci.*, **2012**, *5*: 7833-7853.

[50] Krungleviciute, V.; Lask, K.; Heroux, L.; Migone, A. D.; Lee, J.-Y.; Li, J.; Skoulidas, A. Argon Adsorption on Cu_3(Benzene-1,3,5-tricarboxylate)$_2$(H_2O)$_3$ Metal−Organic Framework. *Langmuir*. **2007**, *23*: 3106-3109.

[51] Yang, Q. Y.; Xue, C. Y.; Zhong, C. L.; Chen, J. F. Molecular simulation of separation of CO_2 from flue gases in Cu-BTC metal-organic framework. *AIChE J*. **2007**, *53*(11): 2832-2840.

[52] Prestipino, C.; Regli, L.; Vitillo; J. G.; Bonino, F.; Damin, A.; Lamberti, C.; Zecchina, A.; Solari, P.L.; Kongshaug, K.O.; Bordiga, Local Structure of Framework Cu(II) in HKUST-1 Metallorganic Framework: Spectroscopic Characterization upon Activation and Interaction with Adsorbates. S. *Chem. Mater*. **2006**, *18*: 1337-1346.

[53] Caskey, S. R.; Wong-Foy, A. G.; Matzger, A. J. Dramatic tuning of carbon dioxide uptake via metal substitution in a coordination polymer with cylindrical pores. *J. Am. Chem. Soc.*, **2008**, *130*(33): 10870-10871.

[54] Prats, H.; Bahamon, D.; Alonso, G.; Giménez, X.; Gamallo, P; Sayos, R. Optimal Faujasite structures for post combustion CO_2 capture and separation in different swing adsorption processes. *J. CO_2 Util*. **2017**, *19*: 100–111.

[55] Queen, W. L., Hudson, M. R., Bloch, E. D., Mason, J. A., Gonzalez, M. I., Lee, J. S., Gygi, D., Howe, J. D., Lee, K., Darwish, T. A.; James, M. Comprehensive study of carbon dioxide adsorption in the metal–organic frameworks M_2(dobdc) (M= Mg, Mn, Fe, Co, Ni, Cu, Zn). *Chemical Science*, **2014**, *5*(12): 4569-4581.

[56] Olson, D. H. The crystal structure of dehydrated NaX, *Zeolites*, **1995**, *15*: 439– 443.

[57] Materials Studio 6.1; Accelrys Inc.: San Diego, CA, **2013**.

[58] Frenkel, D.; Smit, B. *Understanding Molecular Simulation: from Algorithms to Applications*, Academic Press, London, **2002**. ISBN: 0-12-267351-4

[59] Coudert, F.-X.; Boutin, A.; Jeffroy, M.; Mellot-Draznieks, C.; Fuchs, A. H. Thermodynamic Methods and Models to Study Flexible Metal–Organic Frameworks. *Chem. Phys. Chem*. **2011**, *12*: 247–258.

[60] Tan, J. C.; Bennett, T. D.; Cheetham, A. K. Chemical structure, network topology, and porosity effects on the mechanical properties of Zeolitic Imidazolate Frameworks. *Proc. Natl. Acad. Sci. USA* (*PNAS)*. **2010**, *107*: 9938–9943.

[61] Yan, Y.; Lin, X.; Yang, S. H.; Blake, A. J.; Dailly, A.; Champness, N. R.; Hubberstey, P.; Schroder, M. Exceptionally high H_2 storage by a metal–organic polyhedral framework. *Chem. Commun*. **2009**, *7*: 1025–1027.

[62] Watanabe, K.; Austin, N.; Stapleton, M. R. Investigation of the Air Separation Properties of Zeolites Types A, X and Y by Monte Carlo Simulations. *Mol. Simul*. **1995**, *15*: 197-221.

[63] Mayo, S. L.; Olafson, B. D.; Goddard III, W. A. DREIDING: a generic force field for molecular simulations. *J. Phys. Chem*. **1990**, *94*: 8897-8909.

[64] Rappé, A. K.; Casewit, C. J.; Colwell, K. S.; Goddard III, W. A.; Skiff, W. M. UFF, a full periodic table force field for molecular mechanics and molecular dynamics simulations. *J. Am. Chem. Soc*. **1992**, *114*: 10024-10035.

[65] Pham, T.; Forrest, K. A.; McLaughlin, K.; Eckert, J.; Space, B. Capturing the H_2–Metal Interaction in Mg-MOF-74 Using Classical Polarization. *J. Phys. Chem C*, **2014**, *118*(39): 22683-22690.

[66] Jaramillo, E.; Auerbach, S. M. New Force Field for Na Cations in Faujasite-Type Zeolites. *J. Phys. Chem. B*. **1999**, *103*: 9589-9594.

[67] Babarao, R.; Jiang, J. Unprecedentedly High Selective Adsorption of Gas Mixtures in rho Zeolite-like Metal−Organic Framework: A Molecular Simulation Study. *J. Am. Chem. Soc*. **2009**, *131*(32): 11417-11425

[68] Potoff, J. J.; Siepmann, J. I. Vapor–liquid equilibria of mixtures containing alkanes, carbon dioxide, and nitrogen. *AIChE J*. **2001**, *47*: 1676-1682.

[69] Abascal, J. L. F.; Vega, C. A general purpose model for the condensed phases of water: TIP4P/2005. *J. Chem. Phys*. **2005**, *123*: 234505.

[70] Ketko, M. H.; Kamath, G.; Potoff, J. J. Development of an Optimized Intermolecular Potential for Sulfur Dioxide. *J. Phys. Chem. C*, **2011**, *115*(17): 4949-4954.

[71] Bourasseau, E.; Lachet, V.; Desbiens, N.; Maillet, J. B.; Teuler, J. M.; Ungerer, P. Thermodynamic behavior of the CO_2+ NO_2/N_2O_4 mixture: a Monte Carlo simulation study. *J. Phys. Chem B*, **2008**, *112*(49): 15783-15792.

[72] Peng, D. Y.; Robinson, D. B. A New Two-Constant Equation of State. *Ind. Eng. Chem. Fundam*., **1976**, *15*: 59-64.

[73] Vlugt, T. J. H.; García-Pérez, E.; Dubbeldam, D.; Ban, S.; Calero, S. Computing the Heat of Adsorption using Molecular Simulations: The Effect of Strong Coulombic Interactions. *J. Chem. Theory Comput*. **2008**, *4*: 1107–1118.

[74] Wiersum, D.; Chang, J. S.; Serre, C.; Llewellyn, P. L. An adsorbent performance indicator as a first step evaluation of novel sorbents for gas separations: application to metal-organic frameworks. *Langmuir*. **2013**, *29*: 3301-3309.

[75] Samanta, A.; Zhao, A.; Shimizu, G. K. H:, Sarkar, P.; Gupta, R. Post-Combustion CO_2 Capture Using Solid Sorbents: A Review. *Ind. Eng. Chem. Res*. **2012**, *51*: 1438–1463.

[76] Pacciani, R.; Torres, J.; Solsona, P.; Coe, C.; Quinn, R.; Hufton, J.; Golden, T.; Vega, L. F. Influence of the Concentration of CO_2 and SO_2 on the Absorption of CO_2 by a Lithium Orthosilicate-Based Absorbent. *Environ. Sci. Technol*. **2011**, *45*: 7083-7088.

[77] Olajire, A. A. CO_2 capture and separation technologies for end-of-pipe applications – A review. *Energy*. **2010**, *35*: 2610–2628.

[78] Bae, Y.-S.; Snurr, R. Q. Development and evaluation of porous materials for carbon dioxide separation and capture. *Angew. Chem., Int. Ed*., **2011**, *50*: 11586-11596.

[79] Skarstrom, C. W. Method and apparatus for fractionating gaseous mixtures by adsorption, *US Patent* 2944627, **1960**.

[80] Chung, Y.; Na, B. K.; Song, H. K. Short-cut evaluation of pressure swing adsorption systems, *Comput. Chem. Eng*., **1998**, *22*: 637–640.

[81] Chan, Y. N.; Hill, F. B.; Wong, Y. W. Equilibrium theory of a pressure swing adsorption process, *Chem. Eng. Sci*., **1981** 36: 243-251.

[82] Joss, L.; Gazzani, M.; Hefti, M.; Marx, D.; Mazzotti, M. Temperature Swing Adsorption for the Recovery of the Heavy Component: An Equilibrium-Based Shortcut Model, *Ind. Eng. Chem. Res*., **2015**, *54*: 3027−3038.

[83] Chaffee, A. L.; Knowles, G. P.; Liang, Z.; Zhang, J.; Xiao, P.; Webley, P. A. CO_2 capture by adsorption: materials and process development, *Int. J. Greenh. Gas Control*. **2007**, *1*: 11-18.

[84] Riboldi, L.; Bolland, O.; Ngoy, J. M.; Wagner, N. Full-plant analysis of a PSA CO_2 capture unit integrated in coal-fired power plants: post- and pre-combustion scenarios. *Energy Procedia*. **2014**, *63*: 2289-2304.

[85] Huck, J. M.; Lin, L.-C.; Berger, A. H.; Shahrak, M. N.; Martin, R. L.; Bhown, A. S.; Haranczyk, M.; Reuterb, K.; Smit, B. Evaluating different classes of porous materials for carbon capture. *Energy Environ. Sci*. **2014**, *7*: 4132–4146.

[86] Sculley, J. P.; Verdegaal, W. M.; Lu, W. G.; Wriedt, M.; Zhou, H. High-throughput analytical model to evaluate materials for temperature swing adsorption processes, *Adv. Mater*. **2013**, *25*: 3957-3961.

[87] Lin, L.-C.; Berger, A. H.; Martin, R. L.; Kim, J.; Swisher, J. A.; Jariwala, K.; Rycroft, C. H.; Bhown, A. S.; Deem, M. W.; Haranczyk, M.; Smit, B. In silico screening of carbon-capture materials. *Nature Materials*, **2012**, *11*: 633-641.

[88] Vujic, B.; Lyubartsev, A. P. Computationally based analysis of the energy efficiency of a CO_2 capture process. *Chem. Eng. Sci.*, **2017**, *174*: 174–188.

[89] Wilcox, J. Carbon Capture. Ed. Springer. New York, **2012**. ISBN: 1461422140.

[90] Wang, Y.; LeVan, M. D. Adsorption Equilibrium of Carbon Dioxide and Water Vapor on Zeolites 5A and 13X and Silica Gel: Pure Components. *J. Chem. Eng. Data*. **2009**, *54*: 2839–2844.

[91] DeCoste, J. B.; Peterson, G. W.; Schindler, B. J.; Killops, K. L.; Browe, M. A.; Mahle, J. J. The effect of water adsorption on the structure of the carboxylate containing metal–organic frameworks Cu-BTC, Mg-MOF-74, and UiO-66. *J. Mater. Chem. A*, **2013**, *1*: 11922-11932.

[92] Küsgens, P.; Rose, M.; Senkovska, I.; Fröde, H.; Henschel, A.; Siegle, S.; Kaskel, S. Characterization of metal-organic frameworks by water adsorption. *Microporous Mesoporous Mater*. **2009**, *120*: 325-330.

[93] Liang, Z.; Marshall, M.; Chaffee, A. L. CO_2 Adsorption-Based Separation by Metal Organic Framework (Cu-BTC) versus Zeolite (13X). *Energy & Fuels*. **2009**, *23*: 2785–2789.

[94] García-Pérez, E.; Gascón, J.; Morales-Flórez, V. Castillo, J. M.; Kaptejin, F.; Calero, S. Identification of Adsorption Sites in Cu-BTC by Experimentation and Molecular Simulation. *Langmuir*, **2009**, *25*(3): 1725-1731

[95] Peng, X.; Lin, L-C.; Sun, W.; Smit, B. Water Adsorption in Metal–Organic Frameworks with Open-Metal Sites. *AIChE J*. **2015**, *61*(2): 677-687.

[96] Huang, L.; Joshi, K. L.; van Duin, A. C.; Bandosz, T. J.; Gubbins, K. E. ReaxFF molecular dynamics simulation of thermal stability of a $Cu_3(BTC)_2$ metal–organic framework. *Phys. Chem. Chem. Phys.*, **2012**, *14*: 11327-11332.

[97] Canivet, J.; Fateeva, A.; Guo, Y.; Coasnec, B.; Farrusseng, D. Water adsorption in MOFs: fundamentals and applications. *Chem. Soc. Rev.*, **2014**, *43*: 5594—5617.

[98] Burtch, N. C.; Jasuja, H.; Walton. K. S. Water Stability and Adsorption in Metal−Organic Frameworks. *Chem. Rev*. **2014**, *114*: 10575−10612.

[99] Low, J. J.; Benin, A. I.; Jakubczak, P.; Abrahamian, J. F.; Faheem, S. A.; Willis, R. R. Virtual High Throughput Screening Confirmed Experimentally: Porous Coordination Polymer Hydration. *J. Am. Chem. Soc*. **2009**, *9*(131): 15834-15842.

[100] Al-Janabi, N.; Hill, P.; Torrente-Murciano, L.; Garforth, A.; Gorgojo, P.; Siperstein, F.; Fan, X. Mapping the Cu-BTC metal–organic framework (HKUST-1) stability envelope in the presence of water vapour for CO_2 adsorption from flue gases. *Chem. Eng. J.*, **2015**, *281*: 669–677.

[101] Palomino, M.; Corma, A.; Rey, F.; Valencia, S. New insights on CO_2-methane separation using LTA zeolites with different Si/Al ratios and a first comparison with MOFs. *Langmuir*, **2010**, *26*: 1910–1917.

[102] Grajciar, L.; Wiersum, A.; Llewellyn, P.; Cang, J.-S.; Nachtigall, P. Understanding CO_2 Adsorption in CuBTC MOF: Comparing Combined DFT–ab Initio Calculations with Microcalorimetry Experiments. *J. Phys. Chem. C*. **2011**, *115*: 17925–17933.

[103] Joos, L.; Swisher, J.A.; Smit, B. Molecular Simulation Study of the Competitive Adsorption of H_2O and CO_2 in Zeolite 13X. *Langmuir*. **2013**, *29*: 15936−15942.

[104] Myers, A.L.; Prausnitz, J.M. Themodynamics of Mixed Gas Adsorption. *AIChE J*. **1965**, *11*: 121-127.

[105] Krishna, R.; van Baten, J. M. Diffusion of hydrocarbon mixtures in MFI zeolite: Influence of intersection blocking. *Chem. Eng. J.*, **2008**, *140*: 614– 620.

[106] Granite, E. J.; Pennline, H. W.; Photochemical removal of mercury from flue gas, *Ind. Eng. Chem. Res*. **2002**, *41*: 5470-5476.

[107] Peng X, Cao D. Computational screening of porous carbons, zeolites, and metal organic frameworks for desulfurization and decarburization of biogas, natural gas, and flue gas. *AIChE J*. **2013**, *59*: 2928–2942.

[108] D'alessandro, D.; Smit, B.; Long, J. R. Carbon Dioxide Capture: Prospects for New Materials. *Angew. Chem., Int. Ed*. **2010**, *49*: 6058− 6082.

[109] Kumar, R. Pressure swing adsorption process: performance optimum and adsorbent selection. *Ind. Eng. Chem. Res.* **1994**, *33*: 1600-1605.

[110] Ho, M. T.; Allinson, G. W.; Wiley, D. E. Reducing the cost of CO_2 capture from flue gases using pressure swing adsorption, *Ind. Eng. Chem. Res.* **2008**, *47*: 4883-4890.

[111] Zhao, R.; Zhao, L.; Deng, S.; Song, C.; He, J.; Shao, Y.; Li, S. A comparative study on CO_2 capture performance of vacuum-pressure swing adsorption and pressure-temperature swing adsorption based on carbon pump cycle. *Energy*, **2017**, 1-15. DOI: 10.1016/j.energy.2017.01.158.

[112] Choi, W. K.; Kwon, T. I.; Yeo, Y. K.; Lee, H.; Na, B. K.; Song, H. K. Optimal operation of the pressure swing adsorption (PSA) process for CO_2 recovery, *Korean J. Chem. Eng.* **2003**, *20*: 617-623.

[113] Anantharaman, R.; Bolland, O.; Booth, N.; van Dorst, E.; Ekstrom, C.; Sanchez Fernandes, E.; Franco, F.; Macchi, E.; Manzolini, G.; Nikolic, D.; Pfeffer, A.; Prins, M. Rezvani S.; Robinson, L. *European best practice guidelines for assessment of CO_2 capture technologies*. Politecnico di Milano and Alstom UK technical report, **2011**.

[114] Zhang, J.; Webley, P.; Xiao, P. Effect of process parameters on power requirements of vacuum swing adsorption technology for CO_2 capture from flue gas. *Energy Conversion and Management*, **2008**, *49*(2): 346-356.

[115] Nikolaidis, G. N.; Kikkinides, E. S.; Georgiadis, M. C. An Integrated Two-Stage P/VSA Process for Postcombustion CO_2 Capture Using Combinations of Adsorbents Zeolite 13X and MgMOF-74. *Ind. Eng. Chem. Res.* **2017**, *56*(4): 974−988.

[116] Ishibashi, M.; Ota, H.; Akutsu, N.; Umeda, S.; Tajika, M.; Izumi, J.; Yasutake, A.; Kabata, T.; Kageyama, Y. Technology for removing carbon dioxide from power plant flue gas by the physical adsorption method. *Energy Convers. Manage.*, **1996**, *37*: 929–933.

[117] Hefti, M.; Joss, L.; Bjelobrk, Z.; Mazzottia, M. On the potential of phase-change adsorbents for CO_2 capture by temperature swing adsorption. *Faraday Discuss.*, **2016**, *192*: 153-179.

[118] Liu, Z.; Grande, C. A.; Li, P.; Yu, J.; Rodrigues, A. E. Multi-bed vacuum pressure swing adsorption for carbon dioxide capture from flue gas. *Sep. Purif. Technol.*, **2011**, *81*: 307–317.

[119] Leperi, K. T.; Snurr, R. Q.; You, F. Optimization of Two-Stage Pressure/Vacuum Swing Adsorption with Variable Dehydration Level for Postcombustion Carbon Capture. *Ind. Eng. Chem. Res.* **2016**, *55*: 3338−3350.

[120] Tlili, N.; Grévillot, G.; Vallières. C. Carbon dioxide capture and recovery by means of TSA and/or VSA. *Int. J. Greenh. Gas Control*, **2009**, *3*(5): 519- 527.

[121] Plaza, M. G.; Durán, I.; Rubiera, F.; Pevida, C. Adsorption-based process modeling for post-combustion CO_2 capture. *Energy procedia*, **2017**, *114*: 2353-2361.

[122] Zhao, R.; Deng, S.; Wang, S.; Zhao, L.; Zhang, Y.; Liu, B.; Li, H.; Yu, Z. Thermodynamic research of adsorbent materials on energy efficiency of vacuum-pressure swing adsorption cycle for CO_2 capture. *Appl. Therm. Eng.*, **2018**, *128*: 818–829.

[123] Abu-Zahra, M. R. M.; Niederer, J. P. M.; Feron, P. H. M.; Versteeg, G. F. CO_2 capture from power plants: Part II. A parametric study of the economical performance based on mono-ethanolamine. *Int. J. Greenh. Gas Control*, **2007**, *1*(2): 135–142.

[124] Raynal, L.; Alix, P.; Bouillon, P.-A.; Gomez, A.; Le Febvre De Nailly, M.; Jacquin, M.; Kittel, J.; Di Lella, A.; Mougin, P; Trapy, J. The DMX™ process: An original solution for lowering the cost of post-combustion carbon capture. *Energy Procedia*, **2011**, *4*: 779–786.

[125] Singh, P.; Van Swaaij, W. P. M.; Brilman, D. W. F. Energy Efficient Solvents for CO_2 Absorption from Flue Gas: Vapor Liquid Equilibrium and Pilot Plant Study. *Energy Procedia*, **2013**, *37*: 2021–2046.